ROUGHNESS DISCRIMINATION OF TEXTURED GRATINGS USING MULTIPLE CONTACT METHODS

A Thesis

Submitted to the Faculty

of

Purdue University

by

Matthew B. Kocsis

In Partial Fulfillment of the

Requirements for the Degree

of

Master of Science in Electrical and Computer Engineering

August 2011

Purdue University

West Lafayette, Indiana

This thesis is dedicated to my parents Mike and Deb who have supported me with guidance and advice throughout my life.

ACKNOWLEDGMENTS

The author thanks Dr. Hong Tan for the motivation, advice, and background that made this research possible. Thanks to Dr. Tan, Dr. Bernard (Dov) Adelstein, Mike Kocsis, and Deb Kocsis for help revising this thesis as well as the journal and conference paper that this research has produced. Thanks to Dr. David Ebert and Dr. Jan Allebach for serving on the graduate committee to review this work. Thanks also to Steven Cholewiak who helped collect data and discuss results, experimental methods, and future research.

Research presented was supported in part by a National Science Foundation Award under Grant No. 0098443-IIS, and in part by NASA under award No. NCC 2-1363. In addition, the author was partially supported by a graduate fellowship from the School of Electrical and Computer Engineering at Purdue University, and partially supported financially by Rockwell Collins Inc. Appreciation is extended to Drs. Susan Lederman and Roberta Klatzky for discussions on experimental methods, Mike Sherwood at Purdue University for his assistance with the fabrication of the EDM samples with surface gratings, and Patrick Kalita for the spectral analysis of virtual texture gratings.

Portions of this thesis were written in collaboration with Dr. Hong Z. Tan and Dr. Bernard D. Adelstein, and portions of the data presented in this thesis were collected by Ryan M. Traylor and Steven A. Cholewiak. Statistical analysis of resulting data was performed by Bernard D. Adelstein. Profilometer verification of the stainless steel samples was performed by Ryan M. Traylor.

TABLE OF CONTENTS

Page

LIST OF TABLES

LIST OF FIGURES

ABBREVIATIONS

ANOVA	Analysis of Variance
DOF	Degree of Freedom
JND	Just-Noticeable Difference
EDM	Electrical Discharge Machining
n-D	n-Dimensional
FFT	Fast Fourier Transform

ABSTRACT

Kocsis, Matthew B. M.S.E.C.E, Purdue University, August 2011. Roughness Discrimination of Textured Gratings Using Multiple Contact Methods. Major Professor: Hong Z. Tan.

Many studies on texture perception have focused on the perceived roughness of texture samples. The present study continues this analysis by conducting a set of nearly identical amplitude discrimination experiments using three common texture contact methods: fingertip on real gratings (Finger-real), stylus on real gratings (Stylus-real), and stylus on virtual gratings (Stylus-virtual). Two types of textures were used: sinusoidal gratings and triangular gratings that varied along one dimension. Both grating types had a spatial period of 2.5 mm and had the same macro-scale dimensions. The real gratings were fabricated from stainless steel by an electrical discharge machining process while the virtual gratings were rendered via a programmable force-feedback device called the ministick. On each trial, participants compared test gratings with 55, 60, 65, or 70 μm amplitudes (i.e, heights) against a 50-μm reference using a two-interval two-alternative forced-choice paradigm. The results show discrimination thresholds did not differ significantly between sinusoidal and triangular gratings. With sinusoidal and triangular grating data combined, the average (mean $\pm$ standard error) for the Stylus-real threshold (2.5 ± 0.2 μm) was significantly smaller ($p < 0.01$) than that for the Stylus-virtual condition (4.9 ± 0.2 μm). Differences between the Finger-real threshold (3.8 ± 0.2 μm) and those from the other two conditions were not statistically significant. These results demonstrate strengths and weaknesses of different contact methods for discriminating the roughness of small-scale surface features that create a useful basis for further investigation of human texture perception.

1. INTRODUCTION

Haptic texture perception is a fascinating phenomenon that has attracted much research attention since at least 1925 [1]. Haptic rendering and simulation has the potential to contribute to a multimodal perceptual environment that can benefit users from broad backgrounds. Haptic interaction can help improve the ease and effectiveness of many tasks ranging from robotic surgery [2] to remotely flying aircraft [3]. In many ways, haptic texture perception is akin to visual color perception in the sense that there seems to be an infinite variety of textures to the touch, as there are colors to the eyes, in the natural world. What would it take then to manipulate the feel of surface textures as easily as the color of images? Key issues to be resolved are the physical determinants, the perceptual dimensionality, and the neural mechanisms of texture perception [4]. A multidimensional scaling study using seventeen texture patches (sandpaper, velvet, etc.) found that a three-dimensional perceptual space provided a satisfactory representation of perceived similarity judgment data [5]. The dimensions were roughness-smoothness, hardness-softness, and compressional elasticity ("springiness") of the texture surfaces.

This study was conducted to investigate how variation in surface amplitude affects the perception of the surface roughness. Additionally, this study is also part of an ongoing effort to validate a custom-built force-feedback device capable of rendering textures on the order of microns. As with other human senses, understanding the characteristics of texture perception is vital to design and implementation of systems whose purpose is to render haptic environments for both experimentation and manipulation. The result of this study provides data which compares how different contact methods change the perception and discrimination of perceived roughness.

To study the physical determinants and the neural mechanisms of texture perception, texture samples with well-controlled surface features are needed. Of the three

dimensions proposed by Hollins et al. [5], much is now known about the roughness-smoothness dimension. (See [6] for a recent review.) Typical stimuli used for roughness studies include sandpapers with varying grit numbers (e.g., [7]), metal plates with linear grooves (e.g., [8], [9]), and raised dots with controlled height and density (e.g., [10], [11], [12]).

An alternative to the previously mentioned stimuli is to use one-dimensional sinusoidal gratings with controlled amplitude and spatial wavelength, since sinusoidal signals can be viewed as the building blocks of any surface profile. It is however extremely expensive and time-consuming to fabricate high-definition (i.e., high-precision, fine-resolution) sinusoidal surfaces. One known research group has used such stimuli [13], [14]. On the other hand, it is straightforward to render micro-geometric features such as virtual sinusoidal gratings using software-programmable force-feedback devices (e.g., [15], [16], [17]). Haptic interfaces are similarly well-suited for modulating other perceptual features such as hardness/softness and compressional elasticity (e.g., [18], [19]).

Given the time and cost associated with the fabrication of high-definition real surface gratings, it should be more desirable to use virtual textures. Furthermore, it is relatively easy to alter the parameters of the virtual textured surfaces so that more efficient experimental methods such as adaptive procedures can be used. To do so requires that the following two issues be resolved first: 1) What does it mean for real or virtual textures to have "high-definition" sufficient enough for studying human perception of texture? 2) How valid is it to use virtual textures instead of real ones for studying human texture perception?

If the goal is to measure the amplitude detection or discrimination threshold for surface gratings, then the answer to the first question is that the resolution of the textured surfaces needs to be on the order of single microns [13], [14]. Louw et al. found the detection thresholds of real Gaussian profiles to vary from 1 μm to 8 mm from the narrowest (σ: 150 μm) to the broadest (σ: 240 mm) Gaussian-shaped profiles, regardless of whether the shapes were convex or concave [13]. The thresholds were

then converted to equivalent amplitude detection thresholds of sinusoidal gratings by matching Gaussian and sinusoidal profiles with the same maximum slope (cf. [14], Appendix). The estimated thresholds for sinusoidal gratings were approximately 0.64 to 4.99 μm for spatial periods of 2.5 to 10.0 mm ([14], pp. 1266-1267). For amplitude discrimination, Nefs et al. reported a discrimination threshold as small as 2 μm (reference amplitude: 12.8 μm, spatial period: 2.5 mm) for sinusoidal gratings using active dynamic touch [14]. It was also found that amplitude discrimination improved with increasing spatial period (from 2.5 to 10.0 mm). Note that the thresholds summarized above are for direct finger-to-texture contact.

Lederman [9] demonstrated the inadequacy of traditional fabrication techniques for producing surface features of sufficient precision and resolution in haptics research. In that study, aluminum surfaces with square-shaped gratings were fabricated using either a cutting bit or an electrical discharge machining (EDM) technique. The surfaces looked quite different under a scanning electron microscope (see 1.1) and produced different perceived roughness curves as a function of nominal groove width. It was reported that lands and grooves were cut to within 50 and 25 μm of their nominal values with the cutting bit and EDM, respectively. This accuracy was clearly inadequate in light of the single micron detection and discrimination thresholds measured by Louw et al. and Nefs et al. [13], [14], and the different surfaces were indeed judged differently in a magnitude estimation task [7].

In the present study, stainless steel textured surface samples, with better accuracy and resolution, were fabricated by an improved EDM technique. An additional polishing step was applied to ensure the smoothness of the resulting gratings, in order to reduce the influence of friction encountered during exploration of the gratings. The final quality of these real textured surfaces was verified by surface profilometry as described below in Sec. 3.1.

For virtual surface rendering, it should be noted that most commercially available force feedback devices have a position resolution on the order of 10 μm or greater (e.g., the PHANToM by SensAble Technologies has a nominal position resolution of

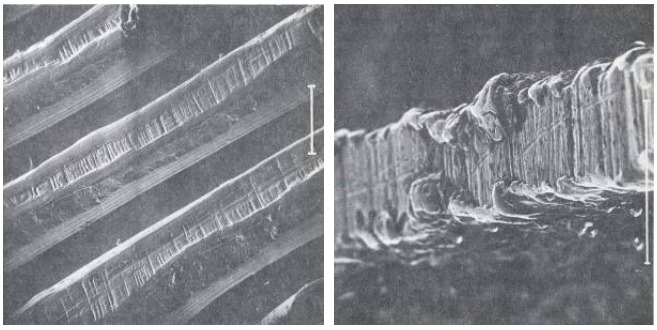

Fig. 1.1.: Scanning electron micrographs of two aluminum plates with grooves created by a cutting bit (left panel; groove width: 0.125 mm, land width: 0.25 mm) and with electrical discharge machining (right panel; groove width: 1.25 mm, land width: 0.25 mm). The vertical white line in each panel represents a length of 200 μm. From Lederman's 1974 study ([9], Figs. 5 and 6).

30 μm; the Omega by ForceDimension has a resolution of 9 μm; both of which are likely the encoder resolution which does not take into account linkage compliance or other factors that further degrade position resolution). In the present study, virtual textures were rendered with a custom-designed 3-DOF (degree of freedom) force-feedback device, the ministick (see Figure 3.6), with verified sensor resolution of 1.5 μm for end-point displacement [20]. The accuracy of the rendered virtual surface gratings was evaluated by recording the stylus positions during lateral stroking and performing a Fourier analysis to examine the spectral components of the surface height profile.

To address the second issue of whether virtual textures can be substituted for real textures for the study of texture perception, discrimination thresholds obtained with real and virtual textures were compared. Ideally, one would prefer to render virtual textures that cannot be distinguished from real textures. It is however almost impossible to demonstrate the equivalence experimentally, short of making interfaces to real and virtual objects that feel, look, and sound identical to participants. Even so, several studies have compared user performance using similar tasks implemented

in real and virtual environments, and the results are mixed. For example, Buttolo et al. [21] reported almost identical task completion time in direct and virtual manipulations. In a study by Unger et al. [22], an interface for a real peg-in-hole task was built to be like the interface to a magnetic levitation haptic device, and it was found that participants performed faster inserting a real peg in a real hole than when using a maglev device with a virtual peg and hole. A further study by Unger et al. [23] found that during a roughness estimation task with virtual textures rendered on a magnetic levitation device, participants showed the same psychophysical function as with a real stylus on real textured surfaces as reported in [24].

Metrics other than task completion time and psychophysical functions have also been employed to compare performance between real and virtual environments. West and Cutkosky [25] asked users to count the number of 1-D sinusoidal cycles on real and virtual surfaces. The best accuracy was found using fingertips on real textured surfaces, followed by a stylus on real textures, with the lowest accuracy for a stylus on virtual textures. Greenish et al. [26] demonstrated that tissue identification accuracy for a real tissue-cutting task was similar to a simulated cutting task in which force data recorded during real cutting were played back through a custom-designed haptic device. More recently, O'Malley and Goldfarb [27] concluded that size-identification tasks performed with a haptic interface capable of sufficient force output can approach the percent-correct level in a real environment, but that the accuracy of size-discrimination tasks performed in a virtual environment was consistently lower than that in a real environment.

Even though results comparing performance in real and virtual environments remain somewhat inconsistent, there is a growing trend of studying haptic texture perception using simulated objects and properties, presumably because it is much easier to create virtual objects than real ones. For example, Ikei et al. showed that a pin-array attached to a force-feedback display enhanced tactile texture perception [28]. Kyung et al. investigated the roles of kinesthetic force feedback, tactile pressure distribution, vibration and skin stretch in displaying surface properties using

an integrated mouse-type haptic display [29]. Campion et al. showed, using a five-bar pantograph-type of haptic display, that both amplitude and friction coefficient of sinusoidal friction gratings contribute to perceived roughness of the gratings [30]. Samra et al. found two diverging patterns of roughness perception using a rotating spiral brush attached to a force-feedback device [31], [32]. Previous studies from Purdue's Haptic Interface Research Lab regarding haptic texture perception have used virtual textures extensively (e.g., [17], [20], [33], [34]).

In order to investigate experimentally whether the ministick can be used as a device to study and reproduce textures, it must be validated against real textures. Since the fundamental purpose of the ministick is for conducting studies of human texture perception, psychophysical experiments were designed to assess how people perceived both real and virtual textures, and then to compare the results directly. The Just-Noticeable Difference (JND), a common psychophysical metric, was used to measure how sensitive human perception is to miniscule differences in textures surfaces. Comparison of the JNDs for both the real and virtual samples can be used as one technique to compare the fidelity of the virtual texture samples. Since real textures are required for the experiments presented in this thesis, psychophysical methods requiring large numbers of samples such as the method of limits and adaptive procedures were not considered practical.

This thesis will present background of texture perception, an experimental study examining perception of real and virtual textures (specific to the roughness-smoothness dimension) rendered on a custom-built device called the ministick, and analysis of the results including observations, explanations, and proposed future work.

2. BACKGROUND

The human sense of touch might be thought by some to be a less important sense, behind sight and hearing. Studies over the past century have shown, however, that the sense of touch is used extensively in daily life; unnoticed to the casual observer. A Study by Klatzky, Lederman, and Metzger found that tactile exploration was actually a remarkably fast and effective method for identifying common objects [35]. Touch itself is not as obvious as it might seem; there are multiple methods of touching an object (static and dynamic, active and passive), as well as multiple types of touch receptors (kinesthetic and cutaneous). The combination of the human nervous system and numerous different types of receptors all over the body all contribute to what is considered one of the five distinct human senses.

2.1 Mechanisms of Touch

At a high level, there are two primary modes of haptic perception: kinesthetic and cutaneous. The kinesthetic system includes muscles and joints and helps the body understand where it is and what position it is in [36]. The kinesthetic system is used to perform large scale tasks such as "extend your arms to make a letter T", or "close your eyes and touch your ears". The cutaneous system works on a much smaller level recognizing sensations such as pressure, vibration, temperature, and textures [36]. The remainder of this chapter will focus on the cutaneous system.

Active and Passive touch both play a large role in cutaneous haptic perception. Active touch involves perception where the observer has control over the movements and mechanics of interaction with an object. Passive touch is the opposite; the observer has no control and receives sensory input without any control. There is

no clear demonstration that either active or passive touch is overall superior; each appears to benefit the observer in different situations [37].

Most mechanisms for cutaneous touch are studied on the underside of the hand because it has one of the highest concentrations of receptors on the body. There are four primary mechanoreceptors found on the hand: Meissner (fast-adapting I), Pacinian (fast-adapting II), Merkel (slow-adapting I), and Ruffini (slow-adapting II). Each of these receptors has different properties and responds to different mechanical stimuli [38]. Fast-adapting receptors are best suited to detect changes in stimuli, such as vibration. Slow-adapting receptors are better suited to detect static stimuli, such as constant pressure. The neurological inputs from all four receptors combine to form the sensation of cutaneous touch. Table 2.1 presents basic properties of each type of receptor.

Table 2.1: Primary cutaneous mechanoreceptors and associated properties. Data from [38]

	Meissner FAI	Pacinian FAII	Merkel SAI	Ruffini SAII
Adaptation	Fast	Fast	Slow	Slow
Reception Area	Small	Large	Small	Large
Relative Skin Depth	Shallow	Deep	Shallow	Deep

2.2 Texture Perception

The perception of textured objects and materials is one of the major areas of research involving the sense of touch. The texture of an object is goverened by its small-scale physical characteristics. The perception of texture, however, is less clear. Unlike several other properties related to touch such as temperature, weight, and global shape, texture perception requires dynamic touch to discern any fine de-

tails [38]. As previously mentioned, Hollins et al. found that texture perception can be sufficiently represented by a three-dimensional perceptual space; roughness-smoothness, hardness-softness, and compressional elasticity [5]. In a similar study, Picard et al. proposed that the number of perceptual dimensions does not exceed four [39]. Although many studies agree on the general number of dimensions, it is difficult to find much agreement on the definition of the dimensions, with the exception of one, roughness-smoothness (harshness) which has been extensively studied.

Many initial studies on roughness of surface textures demonstrated that spatial cues and skin deformation were the primary stimuli that elicited the perception of roughness [9], [40]. A study by Lederman et al. showed that after extended periods of vibration, the fingertip adapts and loses most of the ability to perceive further vibration [41]. The study then went on to demonstrate that roughness perception, however, was not compromised even after the same extended period of vibration. These results support the view that roughness perception using the bare fingertip does not depend on vibration cues. A more recent study separated the spatial-intensive and temporal-intensive cues used during a spatial-frequency discrimination task. The results showed that temporal cues are still essential for discrimination of the spatial-frequency of a texture [42]. Connor et al. conducted studies that proposed that roughness perception had a more complicated neural basis [4]. The results of that study proposed that both spatial and temporal information were used in discriminating roughness; temporal cues were used predominantly when inter-element spacing was below the physical spacing of the slow-adapting (spatial sensing) mechanoreceptors and spatial cues were predominantly used when the inter-element spacing was large enough that the finger had enough resolution to detect both the elements and spaces between elements (ie, not aliased). The argument that vibrations do not contribute significantly to texture perception (or roughness perception) is further questioned when the contact method with the surface is a rigid link (for example, a probe).

Exploration of a textured surface via a probe presents a new set of questions regarding texture perception. The use of a probe limits the data available to per-

ceive textures and roughness; spatial-intensive information is eliminated completely because the skin is no longer deformed by the surface and vibration cues have the potential to be filtered or amplified due to the probe geometry and contact areas. Lederman and Klatzky have done extensive work regarding texture perception through probes [43], [12], [44], [6]. Their series of studies directly compared roughness perception using a bare finger to different contact methods such as probes and sheaths. All studies found that although different, it was still very possible to perceive texture and roughness while using a non-direct contact method. The results show that probe geometry, element spacing, and exploratory speed do affect roughness perception. An interesting result from the studies shows that speed affects roughness less when active touch is used (as compared to passive touch) which leads to the conclusion that the human perceptual system is able to compensate for active traversal speed [12]. Another concern regarding probe-texture interaction is the physical moment of force caused by the distance between the probe's surface and finger contact points. Further studies have shown that the physical moment created by using a probe that extends away from the textured surface is not required to perceive roughness; a zero-moment probe that was designed to eliminate the distance between the grasp point and probe tip was just as effective [6]. These results show promise; although not completely optimal, interaction with textured surfaces via a rigid link is a viable method of texture perception. This conclusion opens the door for virtual and teleoperator rendering and perception of textured surfaces through probes.

2.3 Virtual Rendering

Virtual rendering of haptic textures has enormous potential to change how users interact with distant or artificial environments. Much like virtual or distance communications can render visual or auditory stimulus, virtual haptic rendering would allow for much more immersive communication and better interactive experiences. As with any virtual environment, compromises must be made since anything short of

physically rendering the entire environment would lack some form of realism. Key information needed to create a virtual environment includes determining what is "good enough" for typical human psychophysical perception. Visual systems accomplish this by defining a color gamut, resolution, and frame rate that is deemed acceptable for the type of environment that is being reproduced. Auditory systems use similar compromises, defining how large of a frequency range is needed and what fidelity (bandwidth) is required to successfully transmit and reconstruct sound. In both audio and visual systems, there are vastly different definitions of "acceptable." What works for a telephone call would be completely unacceptable to convey the experience of listening to an orchestra; the fidelity required for an image on the internet might be nowhere near the fidelity needed for a medical imaging device. The first knowledge that is needed to determine these basic requirements is an understanding of the human perceptual system. Only when that system is understood can the correct decisions be made regarding the creation, transmission, and reconstruction of a virtual environment.

Unlike the auditory and visual systems, the human haptic system is spread across the entire body. It is therefore assumed that for most common applications only one part or region of the body would be involved in haptic rendering. For texture perception, highly sensitive areas of the human body are required. Two such areas are the face and hands [38]. For the remainder of this section virtual haptic rendering for perception by the hand will be considered. As noted in chapter 1, defining and studying the perceptual space for haptic texture perception is needed before efficient and well designed virtual haptic environments can be created. There are currently multiple techniques for virtual texture rendering being studied. Some studies have focused on recreating virtual textures that can be directly perceived by the bare finger. This is usually accomplished by designing a grid of pins or air jets that can be directly controlled to render a virtual texture. Shimojo et al. have studied properties of 3-D pin arrays for rendering textures [45] and Bliss et al. studied tactile pattern perception using airjets [46]. Other studies have combined multiple methods of haptic

perception into a single device. A study by Caldwell et al. presented experiments using a multi-modal glove that integrated thermal, vibration, and pressure elements that was able to reasonably reproduce the perception of common surfaces [47].

An additional type of haptic virtual environment is perception through a probe. Although the same limitations demonstrated by using a probe to explore real surfaces and textures would apply to an equivalent virtual environment, there are some benefits to working with such a system. The first benefit of using a probe to explore virtual haptic environments is that there is much existing literature regarding using a probe to interact with real environments. This literature has the potential to aid in the design and validation of virtual systems. A primary disadvantage of perception of a haptic environment through a probe ends up being an advantage when designing virtual probe systems: the probe limits the sensory information available to the user. It is possible when using a virtual probe to replicate the same probe-skin contact that occurs when interacting with real environments; therefore some of the direct stimuli such as skin deformation, temperature, and lateral force on the finger can remain consistent. The disadvantage of this method, however, is that the vibration and force information transmitted through the probe to the fingers and hands must have high fidelity, since they are the primary (or sole) channels for texture perception. Another benefit of this type of interaction is the availability of commercial devices designed for the specific purpose of probe-based haptic perception. The PHANToM by SensAble Technologies and the Omega by ForceDimension are two such devices. There are also numerous custom-built haptic devices for probe-texture manipulation, one of which is called magnetic levitation haptic device developed at Carnegie Mellon University.

When designing any virtual environment, rendering algorithms and techniques must be considered. When rendering a virtual probe for haptic perception, the probe-surface interaction is important to consider. When encountering a stiff surface, a very common technique is to let the probe penetrate the surface and then apply a force that is proportional to the penetration depth [48]. This force can be rendered in several ways; a simple method is to render all force vectors in one dimension that

is tangent to the macro-surface structure (assuming a flat surface), a more complex method is to render the force tangent to the micro-surface structure nearest to the penetration point. Campion and Hayward have studied numerous haptic texture synthesis methods and have presented on their strengths and weaknesses [49]. The effects of friction can also be considered when rendering virtual environments. A study by Campion et al. has shown that friction can influence roughness perception [30]. Another very important rendering consideration when creating virtual probe environments is probe tip geometry. A previously mentioned study by Klatzky and Lederman [44] showed that the probe tip dimensions altered roughness perception for interaction with real textures. Extensive studies have been performed by Unger to better understand virtual rendering techniques relating to probe size and inter-element spacing [50], [23].

3. GENERAL METHODS

A two-interval two-alternative forced choice paradigm based on signal detection theory was used to determine the JND of textures at a certain reference roughness [51]. As previously mentioned, the focus of this study was on one-dimensional gratings because they can be viewed as building blocks of more complex textures since haptic roughness perception has been linked to temporal frequency. Fifty μm was chosen as the amplitude for the reference texture since it is at least one order of magnitude larger than detection thresholds previously reported (eg. [13], [14]). Four experimental conditions were created, each comparing the reference texture with another of increasing roughness. Detection theory was then used to determine the sensitivity or discriminability (noted as d'). Response bias calculations (noted as β) were collected; however they were not used in the formal results.

There are multiple ways to render virtual textures. One of the simplest techniques uses the penetration depth penalty method by applying a restoring force proportional to the penetration depth and in the opposite direction [48]. The models presented in this study use a simple one-dimensional penetration depth penalty model in the z-axis direction (up) for rendering surfaces. Surface geometry was calculated on the fly using probe tip position; equations are presented later in the virtual gratings sections. The probe tip used in these experiments was modeled as a single point.

3.1 Real Gratings

The grating samples used in this experiment were machined out of stainless steel blocks using a wire electrical discharge machining (EDM) process. (See also [14].)

The dimension of each block was 100 mm (Length) × 30 mm (Width) × 15 mm (Height). The high-precision sinusoidal gratings have profiles specified by Eqn. 3.1:

$$h_{sin}(x) = A_{sin} sin(2\pi x l \lambda) \tag{3.1}$$

where h_{sin} denotes the vertical (z) height of the sinusoidal grating surface, x the horizontal position, A_{sin} the grating's sinusoidal amplitude, and λ the spatial period. It is a time-consuming process to fabricate the samples and this experiment was limited to one value of λ (2.5 mm), one reference amplitude (A_0 = 50 μm) and four comparison amplitudes (A_1 = 55 μm, A_2 = 60 μm, A_3 = 65 μm, A_4 = 70 μm). This spatial period corresponds to the inter-element spacing that produced the greatest perceived roughness, according to roughness judgments reported in [6] and [50]. Figure 3.1 shows the sinusoidal grating block with A_3 = 65 μm.

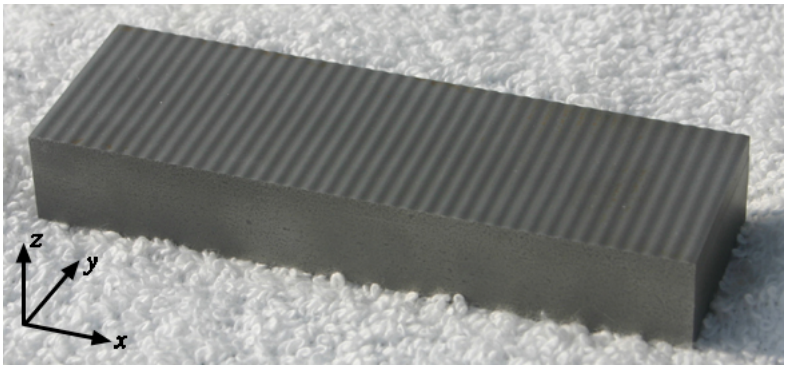

Fig. 3.1.: A stainless steel block with a sinusoidal surface grating
(λ = 2.5 mm, A_3 = 65 μm).

After the sample surfaces were sandblasted clean, a surface profilometer (model Surtronic 3plus, Taylor Hobson, UK) was used to verify the surface geometry of each of the five sinusoidal grating samples at a sampling period of 1 μm. The tip of the profilometer was moved along the length of the block (x-axis) while maintaining contact with the surface. The height trace h(x) along a fixed y position could then be plotted and analyzed. Figure 3.2 shows the h(x) plot for A_3 = 65 μm) and its Fourier transform. It can be seen that the EDM produced a very clean sinusoidal profile with

an amplitude of 65 μm. There were no discernable harmonics at multiples of 400 cycles/m ($\frac{1}{\lambda}$). The side lobes were associated with the sinc function due to the finite sample length of h(x). The profilometer was also used to measure parallel profiles in the x direction along several y values to check the grating consistency along the width of the block (y-axis). The traces were then combined to form a three-dimensional (3D) raster-scan plot of the sinusoidal grating sample shown in Figure 3.3 for $A_3 = 65$ μm. Further Fourier analysis confirmed that the surface profile was consistent along its width. This validation process was repeated for each of the grating blocks.

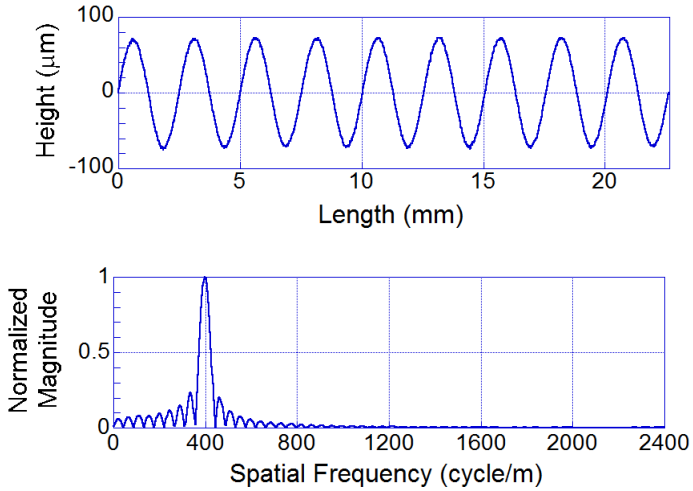

Fig. 3.2.: (Top) Profilometry surface height h(x) of a sinusoidal grating sample ($\lambda =$ 2.5 mm, $A_3 = 65$ μm). (Bottom) Normalized spectral magnitude of the measured height profile in the top panel.

The triangular grating samples were also fabricated from stainless steel blocks by an EDM process. Again, five samples were made with amplitudes (half of peak to trough) that were the same as those of the sinusoidal gratings: $A_0 = 50$ μm (reference), $A_1 = 55$ μm, $A_2 = 60$ μm, $A_3 = 65$ μm, and $A_4 = 70$ μm. They were again calibrated with a surface profilometer. Figure 3.4 shows the height map for

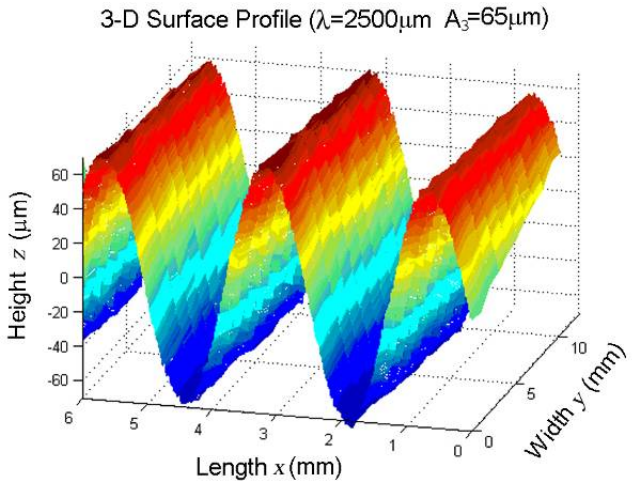

Fig. 3.3.: A 3-D raster-scan plot of the sinusoidal grating surface with a spatial period of 2.5 mm and amplitude of 65 μm (A_3). It shows multiple length-wise profilometer scans taken at several displacements along the width of the grating. (Modified from [24], Fig. 5, ©2010 IEEE)

the 65 μm sample and its Fourier transform. Mathematically, the Fourier series of a triangular waveform is

$$A_{tri}\left(\frac{8}{\pi^2}\right)\left\{sin\frac{2\pi x}{\lambda}+\left(\frac{1}{3}\right)^2 sin3\frac{2\pi x}{\lambda}+\left(\frac{1}{5}\right)^2 sin5\frac{2\pi x}{\lambda}+...\right\} \tag{3.2}$$

Therefore, the spectral components of a triangular profile include its fundamental, a third harmonic with a magnitude that is $\frac{1}{9}$ of that of the fundamental, a fifth harmonic at $\frac{1}{25}$ of the amplitude of the fundamental, etc., as evident in the bottom plot of Figure 3.4. Other than the side lobes around the fundamental component due to the finite signal length, there was no discernable noise in the Fourier spectrum. Multiple traces along the width of the sample were also taken (see Figure 3.5) and the data confirmed that each triangular grating sample was consistent along its width.

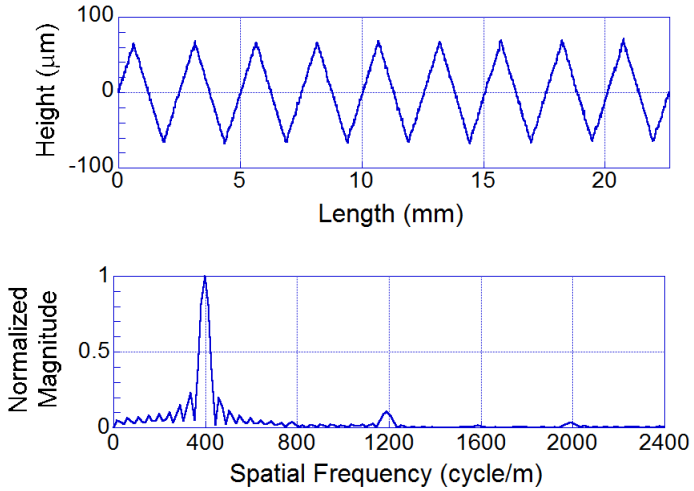

Fig. 3.4.: (Top) Profilometry surface height h(x) of a triangular grating sample (λ = 2.5 mm, A_3 = 65 μm). (Bottom) Normalized spectral magnitude of the measured height profile in the top panel.

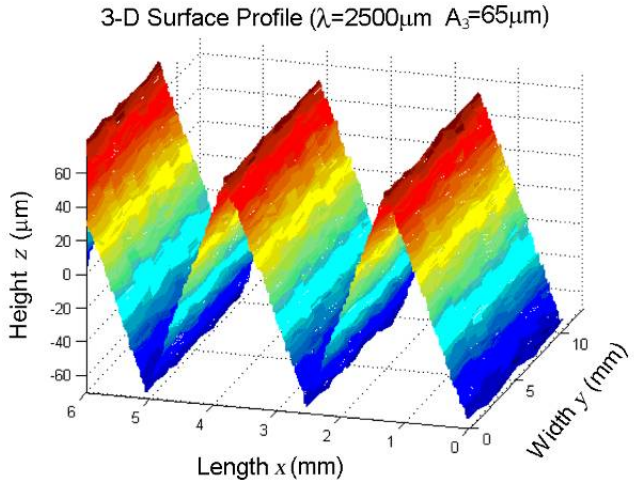

Fig. 3.5.: A 3-D raster-scan plot of the triangular grating surface with a spatial period of 2.5 mm and amplitude of 65 μm (A_3). It shows multiple length-wise profilometer scans taken at several displacements along the width of the grating. (Modified from [52], Fig. 5, ©2010 IEEE)

3.2 Virtual Gratings

The virtual gratings for this study were rendered by a 3-DOF force-feedback device called the ministick [53]. The device is based on the mechanical linkage described by Adelstein [54] and implemented by Steger et al. [55], but with a revised ethernet-enabled embedded controller for stand-alone operation designed and built by Traylor [53]. The ministick has a calibrated position resolution of 1.5 μm [20]. Its force commands are updated at 2 kHz. Figure 3.6 shows a user interacting with virtual haptic objects using a stylus. The height map of the virtual sinusoidal gratings was the same as Eqn. 3.1 where $\lambda = 2.5$ mm and A was selected on the fly from the five amplitude values of 50, 55, 60, 65, or 70 μm. The feedback force was calculated as

$$F_z = \begin{cases} K \times [h(x) - p_z] & \text{when } p_z < h(x) \\ 0 & \text{otherwise} \end{cases} \tag{3.3}$$

where the force F_z always pointed up (i.e., no tangential component F_x or F_y), p_z was the z position of the ministick stylus tip, and the stiffness coefficient K was kept constant at 2.0 kN/m.

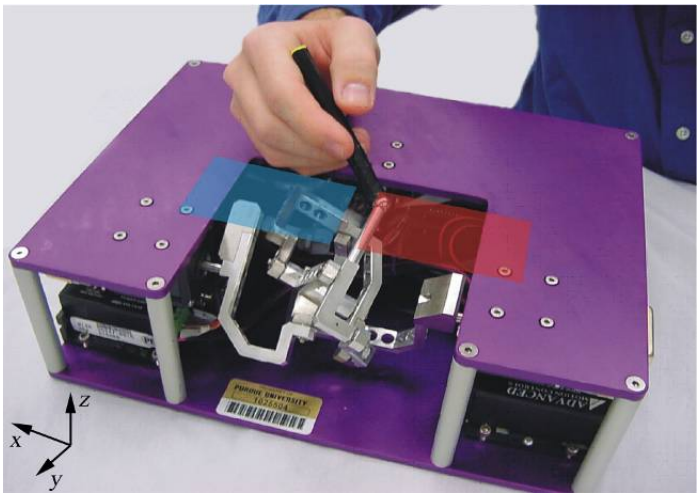

Fig. 3.6.: The ministick force-feedback haptic device. The magenta and cyan patches indicate (roughly) the locations of the virtual textured gratings being discriminated.

The height map of the virtual sinusoidal and triangular gratings were defined by

$$h_{sin}(x) = A_{sin} \times sin(x) \tag{3.4}$$

$$h_{tri}(x) = \begin{cases} \frac{4A_{tri}}{\lambda} x_{mod} - A_{tri} & \text{if } x_{mod} < \frac{\lambda}{2} \\ -\frac{4A_{tri}}{\lambda}\left(x_{mod} - \frac{\lambda}{2}\right) + A_{tri} & \text{if } x_{mod} \geq \frac{\lambda}{2} \end{cases} \tag{3.5}$$

$$\text{where } x_{mod} = x \text{ modulus } \lambda$$

Feedback force was calculated according to the simple penalty-based method outlined by Eqn. (3.3).

The characteristics of the virtual sinusoidal gratings were evaluated by analyzing recorded position signals in the temporal and spatial frequency domains. Specifically, $x(t)$ and $z(t)$ were recorded at a sampling rate of 2 kHz while the user stroked a virtual grating. The Fast Fourier Transform (FFT) of the $z(t)$ data was calculated to show the temporal frequency content of the surface heights traversed by the stylus. In addition, cubic spline interpolation was used to resample $z(t)$ at uniformly spaced x-displacement with a sampling period of Δx = 5 μm. The FFT of $z(x)$ was then taken to examine the spatial frequency contents of the recorded surface height signal. Before the FFT operation, the data points at the beginning and end of a stroke were removed and a 2nd-order polynomial fit was subtracted from the data to remove the low-frequency variations in penetration depths. Figure 3.7 shows an example of the recorded $z(t)$ for one stroke and the corresponding interpolated and de-trended $z(x)$ are shown in the top two panels (a) and (b), respectively. It is apparent that the periodicity of the $z(t)$ waveform is not regular in Figure 3.7(a) presumably due to the non-constant stroking velocity by the user. After re-sampling, the de-trended $\Delta z(x)$ signal in Figure 3.7(b) has a spatial period of 2.5 mm as expected. The bottom two panels of Figure 3.7 show the averaged FFT magnitudes (in dB) from multiple traces of $z(t)$ and $z(x)$, respectively. In Figure 3.7(c), there is a broad spectral peak around 8 Hz, corresponding to an average stroking velocity of approximately 20 mm/s (2.5 mm $\times$ 8 Hz). The breadth of the temporal spectral peak again reflects the variation in stroking velocity. Finally, in Figure 3.7(d), there is a narrower spectral peak at

a spatial frequency of 0.4 cycles per mm which corresponds to $\lambda = 2.5$ mm, with a value of 33.8dB ($A_{sin} = 49.0\mu m$). There was no evidence of harmonics in either Figure 3.7(c) or 3.7(d).

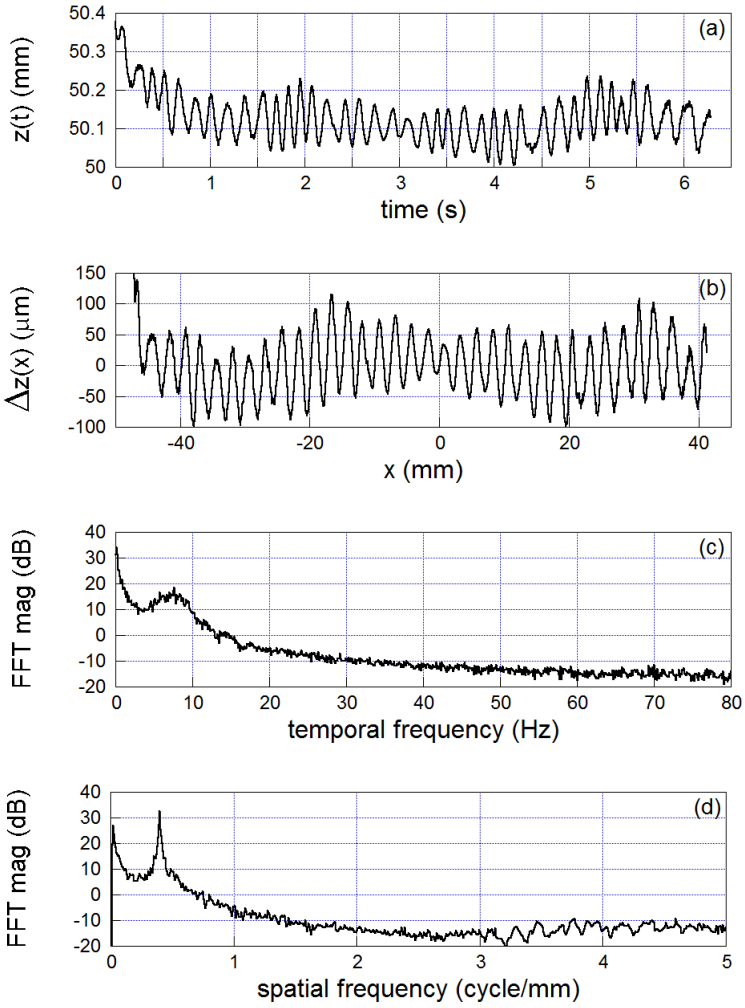

Fig. 3.7.: Analysis of virtual sinusoidal gratings. (a) Recorded temporal position of the stylus z(t) for a sinusoidal grating with $A_0 = 50$ μm and $\lambda = 2.5$ mm. (b) The same signal resampled with respect to x. (c) Temporal FFT magnitude averaged over the FFT of several recordings of z(t). (d) Spatial FFT magnitude averaged over the FFT of several traces of z(x).

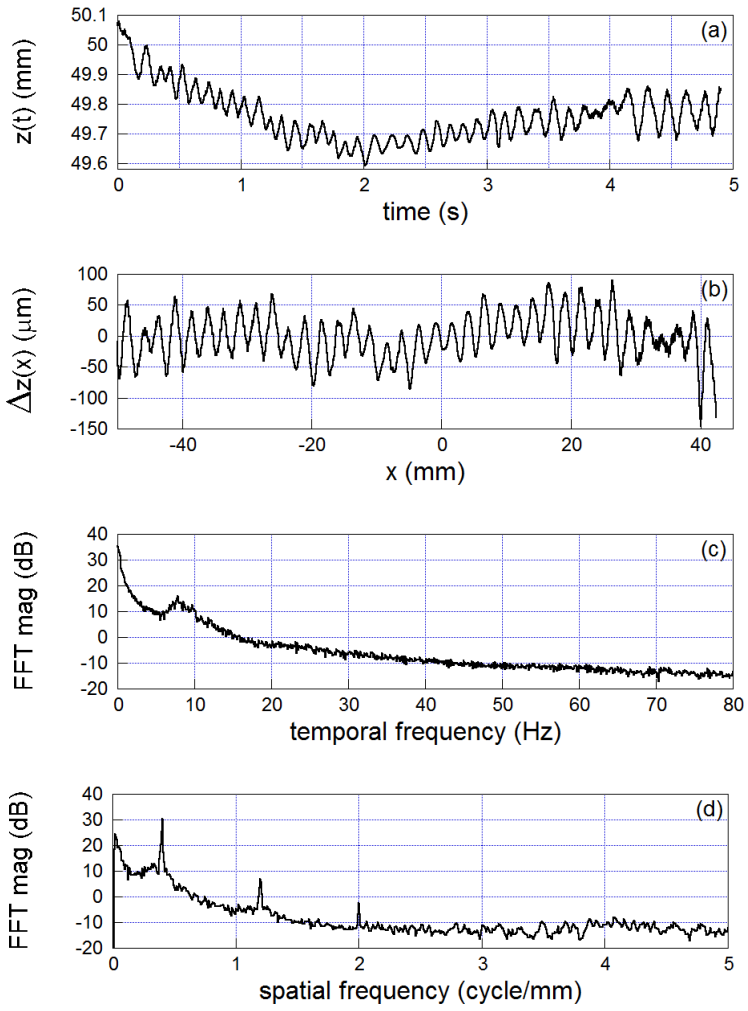

Fig. 3.8.: Analysis of virtual triangular gratings. (a) Recorded temporal position of the stylus z(t) for a triangular grating with $A_0 = 50$ μm and $\lambda = 2.5$ mm. (b) The same signal resampled with respect to x. (c) Temporal FFT magnitude averaged over the FFT of several recordings of z(t). (d) Spatial FFT magnitude averaged over the FFT of several traces of z(x).

The characteristics of the virtual triangular gratings were again evaluated by analyzing recorded position signals in the temporal and spatial frequency domains. Figure 3.8 shows an example of recorded z(t) and the corresponding interpolated and de-trended Δz(x) in the top two panels, respectively. The bottom two panels of Fig-

ure 3.8 show the averaged FFT magnitudes from multiple traces of z(t) and Δz(x), respectively. The difference between the triangular and sinusoidal gratings, indicated by the harmonic components in Eqn. (3.2), is empirically evident in the spatial FFT plotted in Figure 3.8(d). Specifically, the spectral peaks are 31.9 dB ($A_{tri} = 48.6\mu m$) at 0.4 cycles per mm ($\lambda = 2.5mm$), 9.8 dB at 1.2 cycles per mm, and -0.1 dB at 2.0 cycles per mm.

3.3 Procedure

In the presented experiments, amplitude discrimination thresholds were measured with real and virtual sinusoidal and triangular gratings under three experimental conditions: fingertip on real grating (Finger-real), stylus on real grating (Stylus-real) and stylus on virtual grating (Stylus-virtual). Comparisons were made between the JND values obtained with different exploration methods using real textured gratings (Finger-real vs. Stylus-real) and those with real and virtual gratings using the stylus (Stylus-real vs. Stylus-virtual). The results for the sinusoidal Finger-real and Stylus-virtual conditions were presented earlier in a preliminary form in [24]. The results for the triangular Finger-real and Stylus-virtual conditions were reported earlier in a preliminary form in [52].

The experiments followed the two-interval two-alternative forced choice paradigm previously mentioned. Four pairs of grating amplitudes were compared under each experimental condition (Finger-real, Stylus-real and Stylus-virtual): A_0 (50 μm) and A_1 (55 μm), A_0 and A_2 (60 μm), A_0 and A_3 (65 μm), and A_0 and A_4 (70 μm), with A_0 serving as the reference in all pairs. Training and trial-by-trial correct-answer feedback were provided to the participant. A total of 200 trials was collected for each reference-test grating pair. During the experiments, headphone-style hearing protectors (Twin Cup H10A, NRR 29; Peltor, Sweden) were worn by all participants to block possible auditory cues. For the Fingertip-on-real-grating (Finger-real) condition, the participants were instructed to wash their hands with soap and water

to remove residual oils on the skin surfaces. The experimenter and the participant then sat facing each other across a table with a vertical curtain between them. The experimenter inserted two samples into a long slot (see Figure 3.9). A piece of felt fabric with two openings slightly smaller than the grating surfaces (so as to mask the edges) covered the test apparatus. Before starting, it was explained to participants that they would feel two different texture samples and that their task would be to determine which sample felt rougher. Participants placed their dominant hand under the curtain in order to feel the gratings hidden from view. Only the fingertip of the index finger, excluding the nail, was allowed to touch the samples. Participants were free to choose the stroking speed and the amount of time spent touching the samples. Most participants adopted a back-and-forth lateral stroking pattern. For each trial, a computer program determined the presentation location of the two stimuli (reference stimulus on the left or right side). The experimenter spun the test apparatus on the table top several times regardless of whether the order of the stimuli had changed from the previous trial. The experimenter then stopped the apparatus at the desired orientation so that the grating with the higher amplitude was either on the left side (stimulus "1") or right side (stimulus "2") as judged by the participant. The participant verbally responded "One" or "Two" to the experimenter, depending on which side was perceived to have the grating with the higher amplitude. The experimenter then entered the response into the computer. Correct-answer feedback was provided to both the participant and the experimenter by means of two easily discernable audio tones.

Each run comprised a block of 50 trials with the same pair of gratings. The participant took a short break between runs to prevent fingertip numbness. The order of the 16 runs (4 grating pairs $\times$ 4 runs/pair) was randomized for each participant. The experiment was spread over several sessions with each session lasting one to two hours, depending on participant comfort. The procedure for the Stylus-on-real-grating (Stylus-real) condition was identical to that for the Finger-real condition, except that a stylus was used to stroke the gratings as opposed to a fingertip. The

Fig. 3.9.: The test apparatus for holding two stainless steel blocks with surface gratings. The numbers "1" and "2" were used by the experimenter to determine which grating should be presented to the left of the participant on each trial. The apparatus was always obscured by a curtain from the participant's view.

stylus used for this procedure was machined from DelrinTM (Polyoxymethylene) to have the identical look and feel as the one on the ministick (see Figure 3.6). The stylus measured 106 mm in length by 5 mm in diameter that tapered over 13 mm to a 1.6 mm (diameter) hemispherical tip at the end that contacts the grating surface. For the Stylus-on-virtual-grating (Stylus-virtual) condition, the participant stroked two virtual gratings placed side by side with a gap of 12.7 mm (0.5 in) (see the color patches in Figure 3.6). Since it took much less time to present pairs of virtual gratings with the ministick, each run comprised 100 trials. Collection of complete data sets for the virtual-grating condition required, on average, 3 hours per participant compared with 9 hours for the real-grating conditions. Because of the greater time commitment involved, fewer participants were recruited for the Finger-real and Stylus-real conditions. Data collection times for the sinusoidal gratings and the triangular gratings were similar. The order of the 8 runs (4 grating pairs $\times$ 2 runs/pair) was randomized among participants. The participants were instructed to look away from the ministick, but no curtain was used for this condition. The participants themselves directly entered either a "1" or "2" via the computer keyboard based on location of

the grating with the greater perceived height amplitude. Correct-answer feedback was provided by a textual display ("Correct" or "Wrong") on the computer screen.

3.4 Data Analysis

For each participant, a stimulus-response matrix for each grating pair was constructed and the sensitivity index d' and response bias β were calculated based on detection theory [51]. Table 3.1 illustrates how data were captured and defines terms for each of the four outcomes of the two-interval two-alternative force-choice experiments.

Table 3.1: Stimulus-Response Matrix

A_1	Response 1	Response 2
Stimulus 1	Hit	Miss
Stimulus 2	False Alarm	Correct Rejection

$$
\begin{aligned}
\text{Hit Rate } (H) &= P(R1|S1) \\
\text{False Alarm Rate } (F) &= P(R1|S2) \\
d' &= z(H) - z(F) \\
\sigma_F &= \sqrt{\tfrac{F(1-F)}{N_1}} \\
\sigma_H &= \sqrt{\tfrac{H(1-H)}{N_2}} \\
\sigma_{z(F)} &= \sqrt{\tfrac{2\pi F(1-F)}{N_1}} \times e^{\frac{1}{2}[z(F)]^2} \\
\sigma_{z(H)} &= \sqrt{\tfrac{2\pi H(1-H)}{N_2}} \times e^{\frac{1}{2}[z(H)]^2} \\
\sigma_{d'} &= \sqrt{\sigma^2_{z(H)} + \sigma^2_{z(F)}} \\
\beta &= -\tfrac{z(H)+z(F)}{2}
\end{aligned}
\tag{3.6}
$$

The equations in 3.6 were used for each experimental condition to calculate d', $\sigma_{d'}$, and β. It is important to note that neither H nor F can be 0 or 1 in order for the z value

to be well-defined. In the case where H or F were 0 or 1 (in this instance, meaning 100% correct or 100% incorrect responses for a given stimulus), a slight adjustment was made by adding an artificial Hit/Miss or False Alarm/Correct Rejection. See Appendix A for boxes containing "0*" which indicate that this adjustment was made. For the data analysis contained in this study, the only corrections of this nature that were required were conditions where a participant responded with 100% accuracy. Therefore the only required adjustments were to add one artificial Miss or False Alarm where necessary.

$$\alpha = \frac{\frac{d'_1}{5} + \frac{d'_2}{10} + \frac{d'_3}{15} + \frac{d'_4}{20}}{4} \tag{3.7}$$

To estimate the amplitude discrimination threshold (JND) from d' values, the slope of the best-fitting line was calculated by averaging the slopes from the d' values corresponding to the four grating pairs: where d'_i, the sensitivity index for the discrimination of A_0 and A_i (i = 1, 2, 3, 4), was divided by the respective difference between the reference and test grating amplitudes, $\Delta A_i = A_i - A_0$, and then averaged. See equation 3.7 for a complete expression for this calculation. The Just-Noticeable Difference (JND) was then calculated as the amplitude difference $\Delta A = A - A_0$ for which $d' = 1$, or equivalently, $JND = \frac{1}{\alpha}$ (see also [56]). This process is illustrated in Figure 3.10. In the case where a participant's performance saturated (defined by having at most one false alarm and one miss among the 200 trials for a given texture pair), any data for "easier" pairs (those having a larger difference in amplitude) were not included in the calculation. In those cases the equation would simply drop off the final terms and the overall scaling would be changed to take into account the number of conditions included. For example, if the participant saturated with the A_3 condition, the d'_4 term would be dropped and the denominator would be changed to 3. See Appendix A for boxes containing "-" entries which indicate that the experimental condition was not used in JND calculations. It is important to note that one Participant, P16 was deemed to have saturated at A_3 with 3 Misses and 0 False Alarms. This was decided because the participant's results for A_4 were slightly worse

than A_3; these results were judged to be due to concentration and the desensitization of the participant's fingerpad.

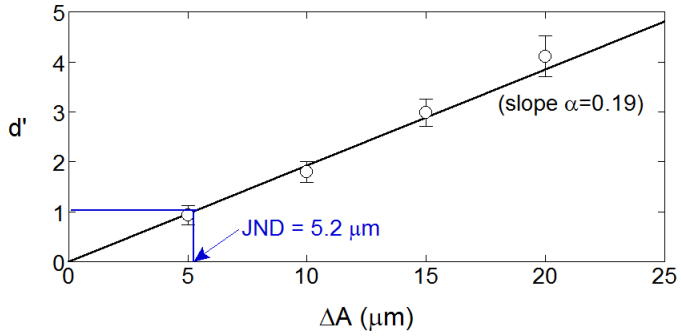

Fig. 3.10.: Illustration of data processing scheme using fictitious data. The d' values ($\pm$ std. err.) associated with the four grating pairs, plotted against ΔA, the amplitude difference between a pair of gratings, are shown. The best fitting line, its slope and estimated amplitude JND are also shown.

4. DISCRIMINATION OF SINUSOIDAL GRATINGS

Sinusoidal Gratings were used in a set of experiments under all three previously mentioned contact methods (Finger-real, Stylus-real, and Stylus-virtual). Sinusoidal gratings were used because they can be thought of as building blocks for textures with more complex profiles via fourier decomposition. Since it is known that vibration is a primary method of amplitude roughness perception, the sinusoidal conditions can be thought of as a baseline where there is only one spatial frequency present. This chapter includes the details and outcomes for the three sinusoidal grating experiments.

4.1 Participants

Fifteen individuals (P1-P15) participated in Experiment 1. Four (2M/2F) took part in the Finger-real condition, four (2M/2F) in the Stylus-real condition, and seven (3M/4F) in the Stylus-virtual condition. All participants except for one (P5) were right-handed and all reported no known conditions that would compromise their sense of touch. Three participants (P1, P2, P10) were laboratory research staff who had previous experience with haptic studies. The rest of the participants were compensated for their time.

4.2 Stimuli

The stimuli for the sinusoidal grating experiments are fully defined in chapter 3. Depending on contact method, real stainless-steel sinusoidal textures and virtual sinusoidal textures rendered by the ministick were used.

Table 4.1: Amplitude Discrimination Thresholds (in μm) by Experimental Condition for Sinusoidal Gratings

Participant	(a) Finger-real	(b) Stylus-real	(c) Stylus-virtual
P1	4.1	-	-
P2	4.4	-	-
P3	4.3	-	-
P4	2.8	-	-
P5	-	3.5	-
P6	-	1.9	-
P7	-	2.7	-
P8	-	1.6	-
P9	-	-	4.9
P10	-	-	5.8
P11	-	-	5.1
P12	-	-	4.5
P13	-	-	4.1
P14	-	-	4.3
P15	-	-	5.3
Average	3.9	2.4	4.9
Std. Err.	0.4	0.4	0.2

4.3 Results

The amplitude discrimination thresholds for all 15 participants under the sinusoidal grating conditions are shown in Table 4.1. The participants' average thresholds (mean $\pm$ standard error of mean) for a reference amplitude of 50 μm under the Finger-real, Stylus-real and Stylus-virtual conditions, respectively, were 3.9 $\pm$ 0.4, 2.4 $\pm$ 0.4 and 4.9 $\pm$ 0.2 μm.

With a complete independent-groups design, the parametric one-way ANOVA (Analysis of Variance) showed that the experimental interface condition had a significant effect ($F_{2,12} = 15.192$, $p < 0.001$) on discrimination thresholds for sinusoidal gratings. Post-hoc Newman-Keuls contrasts indicated that this effect was due to the Stylus-real thresholds being significantly smaller than those for either the Stylus-

virtual (critical difference = 1.57 μm, $p < 0.01$) or Finger-real (critical difference = 1.08 μm, $p < 0.05$). The thresholds for the Stylus-virtual and Finger-real conditions, however, were not significantly different from each other. Because Gaussian tendency of the threshold data cannot be ascertained from our small sample size, a nonparametric (i.e., distribution-free) test was used to corroborate this finding. The Kruskal-Wallis test for independent groups again indicated that the experimental condition had a significant effect ($\hat{H}_{447} = 9.953$, $p < 0.01$). Nonparametric (Kruskal-Wallis) post hoc contrasts, however, showed that only the Stylus-virtual and Stylus-real thresholds differed significantly from each other ($p < 0.01$). Therefore, it is concluded that the detection thresholds for sinusoidal gratings differ significantly only between the real and virtual stylus conditions but conclusions are not drawn for contrasts involving the Finger-real condition.

4.4 Discussion

These results show that the participants were best able to discriminate roughness between two sinusoidal textures when using a rigid stylus on a real texture. The sinusoidal gratings were less discernable using direct finger contact, and least discernable when using a virtual stylus. Although the results for the virtual stylus condition were somewhat expected due to evidence that feeling through a probe often offers fewer cues for perception, the results that the real stylus performed the best were somewhat unexpected. Further discussion is presented in chapter 6 where data from both sinusoidal and triangular experiments are analyzed.

5. DISCRIMINATION OF TRIANGULAR GRATINGS

Triangular Gratings were used in a set of experiments under all three previously mentioned contact methods (Finger-real, Stylus-real, and Stylus-virtual). Triangular gratings were used because they have more spectral complexity than sinusoidal gratings. In addition to gathering basic data on amplitude-based roughness perception using basic sinusoidal gratings, triangular gratings were used to determine whether or not perception of the gratings roughness differences changed as compared to the sinusoidal gratings. This chapter presents the details and results for the three triangular grating experiments.

5.1 Participants

Thirteen different participants were recruited for Experiment 2. Four (2M/2F) took part in the Finger-real condition, four (2M /2F) in the Stylus-real condition, and five (3M/2F) in the Stylus-virtual condition. All participants were right-handed and reported no known conditions that would compromise their sense of touch. Four participants (P18, P19, P20, P24) were laboratory research staff who had previous experience with haptic studies. The rest of the participants were compensated for their time.

5.2 Stimuli

The stimuli for the triangular grating experiments are fully defined in chapter 3. Depending on contact method, real stainless-steel triangular textures and virtual triangular textures rendered by the ministick were used.

Table 5.1: Discrimination Thresholds (in μm) by Experimental Condition for Triangular Gratings

Participant	(a) Finger-real	(b) Stylus-real	(c) Stylus-virtual
P16	3.7	-	-
P17	4.2	-	-
P18	4.1	-	-
P19	2.8	-	-
P20	-	2.1	-
P21	-	2.4	-
P22	-	2.7	-
P23	-	3.1	-
P24	-	-	3.0
P25	-	-	5.7
P26	-	-	6.1
P27	-	-	4.6
P28	-	-	4.8
Average	3.7	2.6	4.8
Std. Err.	0.3	0.2	0.5

5.3 Results

The amplitude discrimination thresholds from all thirteen participants for triangular gratings are shown in three panels for the three grating-stylus conditions in Table 5.1. The participants' average thresholds for the Finger-real, Stylus-real and Stylus-virtual conditions, respectively, were 3.7 $\pm$ 0.3, 2.6 $\pm$ 0.2 and 4.8 $\pm$ 0.5 μm with respect to a 50-μm reference amplitude.

The parametric one-way independent-groups ANOVA showed that the experimental interface condition had a significant effect ($F_{2,10} = 7.468$, $p < 0.02$) on thresholds for triangular gratings. Post-hoc Newman-Keuls contrasts indicate that this effect was due to the Stylus-virtual thresholds being significantly greater than those for the Stylus-real condition (critical difference = 2.09 μm, $p < 0.01$). The other two possible threshold pairings according to interface were not significantly different from each other. The nonparametric Kruskal-Wallis test for independent groups again in-

dicated that the experimental condition had a significant effect ($\hat{H}_{445} = 7.596$, $p < 0.05$), while nonparametric post hoc contrasts supported the finding that only the Stylus-virtual and Stylus-real thresholds differed significantly ($p < 0.01$). Thus, for triangular gratings, it is concluded that the real and virtual stylus conditions differ significantly and conclusions are not drawn for contrasts involving the Finger-real condition.

5.4 Discussion

These results again show that the participants were best able to discriminate roughness between two sinusoidal textures when using a stylus on a real texture. The triangular gratings were less discernable using direct finger contact, and least discernable when using a virtual stylus. The results from the triangular gratings follow the same pattern as the results from the sinusoidal gratings, which is somewhat expected since the one-dimensional gratings are similar (physical size and spatial-period), and since both sinusoidal and triangular gratings will produce similar temporal cues as shown by the fourier decomposition of the texture profiles. Further discussion is presented in chapter 6 where data from both sinusoidal and triangular experiments are analyzed and can be directly compared.

6. SUMMARY

The individual and average threshold results from both experiments are summarized in Figure 6.1. Visual inspection indicates that while thresholds differed across the three experimental conditions, there was little difference between the sinusoidal and triangular gratings.

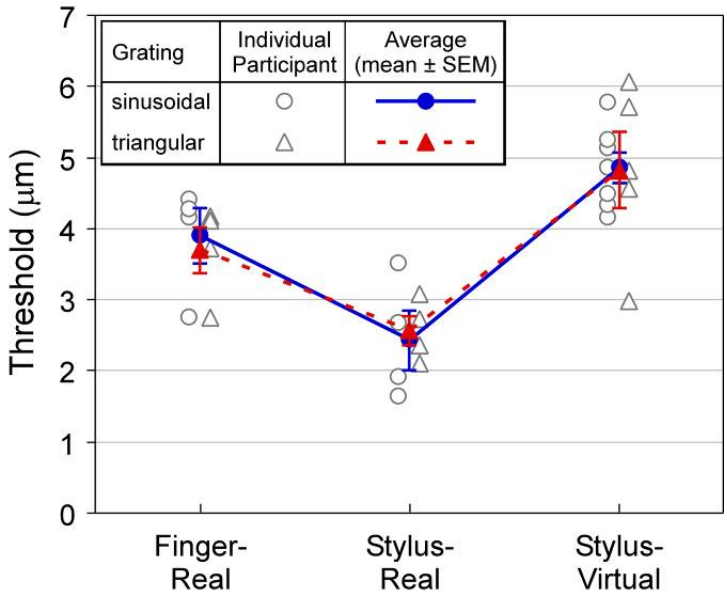

Fig. 6.1.: Comparison of amplitude discrimination thresholds for sinusoidal (open circles) and triangular gratings (open triangles) under the three experimental conditions. Each symbol represents one individual participant's threshold. The average thresholds are shown with filled symbols and are slightly offset for clarity.

Data from the sinusoidal and triangular gratings experiments were pooled for a two-way independent-groups ANOVA. The ANOVA reveals a significant main effect for experimental interface condition ($F_{1,22} = 21.18; p < 0.0001$). Neither the grating type ($F_{2,22} = 0.011; p < 0.916$) nor the interaction between grating type and experimental condition ($F_{2,22} = 0.091; p < 0.913$) were significant. When combined across the sinusoidal and triangular grating profiles, the average discrimination thresh-

olds for the Finger-real (3.8±0.2 μm), Stylus-real (2.5±0.2 μm), and Stylus-virtual (4.9±0.2 μm) conditions all differed significantly ($p < 0.01$) from each other according to Newman-Keuls post-hoc contrasts (Finger-real vs. Stylus-real, critical difference 1.10 μm; Stylus-real vs. Stylus-virtual, critical difference 1.16 μm; Finger-real vs. Stylus-virtual, critical difference 1.01 μm). While the Kruskal-Wallis non-parametric test supports the observation of a significant main effect for experimental condition for the combined sinusoidal and triangular data ($H_{8812} = 18.87, p << 0.01$), the accompanying nonparametric post hoc analysis indicates, however, that only the real and virtual stylus condition thresholds differed significantly ($p < 0.01$).

The average discrimination thresholds for the Finger-real condition were 3.9 μm and 3.7 μm, or 7.8% and 7.4% of the reference amplitude of 50 μm, for sinusoidal and triangular gratings, respectively. The results can be compared directly with that obtained by Nefs et al. [14] where similar stimuli and methods were used. Specifically, they found a discrimination threshold of 8 μm for sinusoidal gratings with a reference amplitude of 51.2 μm and a spatial-period of 2.5 mm. The relatively lower threshold found in the present study may be the result of a small difference in the instructions given to the participants. In the Nefs et al. [14] study, the participants could only stroke the textured surfaces twice from side to side, whereas in the present study participants were allowed to stroke the surfaces as many times as they wished. In pilot tests for the present study, participants were limited to two strokes, but they found the task to be too difficult to perform. Procedures were updated to let the participants feel the textures for as long as needed to measure the best achievable thresholds (personal communications with R. Klatzky and S. Lederman, 2004). A second difference is the use of feedback. In Nefs et al.'s study [14], feedback was given only during practice trials. In the present study, trial-by-trial correct-answer feedback was provided throughout the main experiment. Therefore, the 3.9 μm and 3.7 μm results from the Finger-real condition can be viewed as a lower-bound threshold for amplitude discrimination of sinusoidal and triangular gratings with a 50 μm amplitude and a 2.5 mm spatial period. The 8 μm value from Nefs et al. [14] can be

considered a typical threshold for amplitude discrimination of similar sinusoidal (51.2 μm amplitude) gratings.

6.1 General Discussion

In the Stylus-real condition, average discrimination thresholds were 2.4 μm and 2.6 μm, or 4.8% and 5.2% of the reference amplitude of 50 μm for the sinusoidal and triangular textures, respectively. The finding, that amplitude discrimination thresholds for texture gratings were marginally (i.e., by parametric but not by nonparametric statistical analyses) larger for the Finger-real condition than for the Stylus-real condition, is perhaps counterintuitive considering the fact that more information is available through direct fingerpad exploration than probe-mediated exploration of textures [11], [12]. The real textures, when explored with the bare finger, convey spatial (size of microstructure) and intensive (depth of microstructure) information as well as temporal (vibration) information arising from the lateral stroking of the grating. During normal active touch (i.e., during volitional limb movement), observers rely mainly on spatial-intensive information and can ignore vibratory frequencies to judge texture intensity (i.e., roughness). The virtual texture, on the other hand, can only be experienced via the mechanical vibration of the haptic interface linkage produced by the interaction between the stylus's virtual tip and texture as the grating is stroked. As is the case for exploring the real textures with a rigid stylus, observers can make use of vibratory sensations caused by stylus-grating interaction in conjunction with the kinesthetic feedback from their movement to judge texture intensity. One might thus expect that the thresholds for the Finger-real condition be lower than those for the Stylus-real condition. However, for the reasons stated in the previous paragraph, sensory desensitizing/adaptation might have played a bigger role in the Finger-real condition than in the Stylus-real condition.

There may be several reasons why the thresholds obtained with stylus are lower than those obtained with fingerpad using real texture samples. First, even though care was taken to ensure breaks between runs in the Finger-real condition, it was still

possible that the fingerpad was getting slightly de-sensitized from the repeated rubbing against the stainless steel surfaces. Second, the contact area between the stylus and the hand with the Stylus-real condition was spread across the fingerpads of the thumb, index and middle fingers, resulting in a larger total contact area for detection of temporal vibration patterns. Previous studies have shown that larger contact area can lead to lower thresholds (e.g., [57], [58]). Third, according to anecdotal notes, the Stylus-real condition led to "crisper" or "sharper" sensations than the Finger-real condition. The strong vibrations transmitted by the probe from stroking the textured surfaces might have made it easier to discriminate the roughness of a pair of textures. A possible explanation for this sensation is a damping effect of the soft tissue of the fingertip, compared to the rigid stylus. Potential further research on this topic will be proposed later.

In the Stylus-virtual condition, average amplitude discrimination thresholds of 4.9 μm and 4.8 μm (9.8% and 9.6% of the reference amplitude of 50 μm) were found for the sinusoidal and triangular textures, respectively. These values can be compared to results from a series of experiments on haptic texture perception using force-feedback devices [15], [16], [59], [60], [61], [62]. Our Stylus-virtual sinusoidal condition is similar to Weisenberger and Krier's study [59] where 2-D sinusoidal "bumps" were simulated on a PHANToM force-feedback device. They estimated amplitude JNDs over a range of amplitude and spatial frequency values. For gratings with a spatial frequency of 3.88 cycles/cm, which is close to the 2.5 mm (4 cycles/cm) wavelength of the present study of 1-D gratings, they found JNDs of roughly 0.15 mm (25-12.5% of the reference) for a 0.6-1.2 mm reference amplitude range. Thus, even though Weisenberger and Krier's [59] stimulus amplitudes were 10-20 times larger than those presented in this study, when expressed as Weber fractions, this study's results for the Stylus-virtual condition and their smaller Weber fractions are roughly comparable considering the many differences in stimuli, apparatus and experimental procedures between the two studies.

A possible explanation for the better performance in the Stylus-real condition than that in the Stylus-virtual condition is the difference in surface stiffness. Touching of real and virtual surfaces is inherently different. Specifically, a real stainless steel surface has an almost infinite stiffness and cannot be penetrated by the stylus, whereas a penalty implementation of a virtual surface has a limited stiffness and must be penetrated by a virtual stylus before it can be perceived. The latter results in movement profiles that "drift" in the height direction (z-axis) of the grating profiles (see Figure 3.7b and 3.8b). This might have affected the participants' ability to discriminate the amplitudes of pairs of sinusoidal or triangular gratings as effectively in the Stylus-virtual condition as in the Stylus-real condition. Another factor is that, unlike the real textures, the method employed in this study for rendering both virtual sinusoidal and triangular gratings, expressed by Eqn. 3.3 offers limited resistance to surface penetration and no lateral friction. Although the primary purpose of this research was to determine how amplitude of small-scale textures influences roughness perception, it is known that friction also contributes to roughness perception [30]. Although the amount of friction differed between all three contact methods, it is important to note that it was consistent for any pair-wise discrimination task; therefore different amounts of lateral friction should not influence the discrimination threshold under any single contact method. In light of the many differences between the experiments on real and virtual textures, the thresholds are actually remarkably similar (i.e., within a factor of 2). Future studies could investigate this issue further by increasing the stiffness constant used in the rendering algorithm.

Regardless of the experimental interface condition, the discrimination thresholds obtained for the sinusoidal and triangular gratings were not statistically distinct. There are two possible explanations for this finding. One possibility is that the spatial harmonic components of the triangular gratings were not sufficiently strong to contribute to the perception of a triangular grating. Thus the triangular gratings used in the present study felt like sinusoidal gratings and one would expect similar amplitude discrimination thresholds for both types of gratings. This turned out

not to be the case because the third harmonic component of a 50-μm triangular grating has an amplitude of $50 \times (\frac{8}{\pi^2}) \times (\frac{1}{3})^2 = 4.5\mu m$ at a spatial frequency of 1.2 cycles per mm. This is above the detection threshold of 1.9 μm for a sinusoidal component at a similar spatial frequency of 1.25 cycles per mm reported in [20]. Therefore, the findings of [20] would have predicted that the triangular gratings used in the present study do feel different from the sinusoidal gratings used in the present study. Since in this study participants never directly compared the two gratings, roughness perception data specifically comparing sinusoidal and triangular gratings is not available. A second explanation is that the differences in the amplitudes of the harmonic components of the triangular gratings used in the present study, whether they were real or virtual, were below human discrimination thresholds and therefore did not contribute to the overall amplitude discrimination task for triangular gratings. There are no experimental data available at this time to assess the second explanation.

Klatzky and Lederman [44] demonstrated that participants perceived raised dot textures with smaller interelement (i.e., dot) spacing as being rougher when experienced with a smaller than a larger diameter probe tip, and least rough with the bare finger tip. As inter-element spacing was increased, however, the ordering of perceived roughness by probe sizes and fingertip was reversed. Equating inter-element spacing between raised dots with the spacing between this study's textures' ridges would indicate that the crossover in Klatzky and Lederman's roughness ordering occurred approximately at the wavelength of this study's sinusoidal and triangular gratings. While increased subjective roughness ratings in Klatzky and Lederman's study can be expected to correspond to higher sensitivity and lower threshold, predicting whether the finger or stylus should produce smaller thresholds in the present experiments is difficult for two reasons. First, as noted above, there is a probe tip diameter dependent crossover in roughness ratings [12], [44], suggesting that threshold magnitudes should be comparable for the finger and probe (stylus) near the wavelength of the textures used for these experiments. Second, the probe tip in the present study's Stylus-virtual condition is modeled as a simple point that has zero diameter. Extrap-

olating from the two probe tip diameters in Klatzky and Lederman's study [44], one might expect the roughness rating crossover point to shift to a lower inter-element spacing than the present grating wavelength. Such a shift would make the perceived roughness greater and, therefore, the threshold lower for the finger than for the virtual probe. From the present study, conclusions finding a statistically significant difference between the thresholds obtained with the bare fingertip and those with the stylus cannot be drawn. Therefore, the presented results do not contradict the findings of Klatzky and Lederman [44].

Finally, a main motivation of the present study was to investigate the validity of virtual gratings in studying human texture perception. A recent study by Unger et al. [23], using a six-axis magnetic levitation haptic device for virtual textured haptic surfaces, demonstrated similar psychophysical functions for roughness magnitude estimation for real and virtual textures when probe geometry and velocity were taken into account in the virtual texture model. The results of the present study indicate a two-fold difference between the amplitude discrimination thresholds obtained with a stylus on real gratings (2.5 μm) and those on virtual gratings (4.9 μm). The larger thresholds associated with the virtual gratings could be due to the limited stiffness of the virtual surfaces that resulted in variable peak-trough distances traveled by the probe (see Figure 3.7b and Figure 3.8b; cf. Figure 3.2 top and Figure 3.4 top, respectively) when stroking the virtual gratings. Also, as noted above, this study's virtual textures did not provide tangential resistance forces (i.e., parallel to the stroke direction). Furthermore, even though every effort was made to use the same psychophysical testing protocol with both real and virtual surfaces, it appeared that the participants put in more effort with real texture gratings when the experimenter presented and recorded every trial and the correct-answer feedback signal could be heard by both the experimenter and the participant. Overall, the threshold values obtained in the present study are rather similar considering the many differences among the three experimental conditions of Finger-real, Stylus-real and Stylus-virtual.

The presented results should be viewed in the context of the specific conditions conducted in the present study. For example, this study focused on the perception of surface roughness due to grating amplitudes. It is known that friction (or stickiness) also plays an important role in haptic texture perception [5], [30]. Future work needs to carefully assess the extent to which lateral force profiles can be successfully simulated with a haptic device. In addition, the gratings used in the present study do not reflect the complexity of surface textures encountered in daily life. Other factors, such as surface stiffness and thermal properties, all need to be taken into account when studying haptic texture perception.

6.2 Future Work

During the planning, execution, and analysis phases of these experiments, many new ideas, thoughts, and future improvements were noted. This section will discuss several further studies as well as improvements that could be considered when designing new studies. These further experiments and improvements are not meant to detract from the results presented in this thesis; they are rather a collection of lessons learned and areas for further research that could be studied at a later time.

6.2.1 Method Improvements

During execution and analysis of the presented experiments, several improvements were identified that would be of possible benefit to the data and analysis. The most obvious improvement, from an experimental standpoint, is to take the additional step of maintaining consistency of the experimental conditions throughout the three experimental conditions (Finger-real, Stylus-real, Stylus-virtual). Updating the procedure of the virtual texture experiment to include a curtain and experimenter feedback has the potential to further reduce any participant bias due to concentration or the ability to see the ministick. Another improvement for further experiments is to maintain a consistent set of participants across all experimental methods. This change would

allow for further statistical analysis among experimental conditions within individual participants.

6.2.2 Virtual Rendering Improvements

An area for further studies using the ministick discussed during the analysis of the data presented in this thesis is advanced virtual rendering techniques. There is an inherent limitation of the ministick to three degrees of freedom; however rendering techniques including tangential forces and friction could be implemented and studied. It is understood that lateral forces do play a role in texture perception [16], supporting additional investigation into mechanisms to virtually render more complex forces. Probe tip rendering has also been shown to have effects on virtual texture rendering [23], and even though the sinusoidal textures in the present study were not too narrow for the probe size used, the triangular textures (as well as other further complex textures) could potentially be rendered differently when considering both probe diameter and multiple surface contacts. For example a spherical probe placed at the bottom of steep triangular trough would experience multiple tangential forces from both sides of the trough.

6.2.3 Advanced Data Recording

Analysis of the virtual probe data (presented in figures 3.7 and 3.8) opens questions regarding how the real texture samples are traversed. The real textures were validated with profilometer data; however experimental traversal data were not recorded. Would there be a way to measure damping effects caused by using the pad of the finger to perceive the surface? Does using a stylus amplify vibrations caused by traversing the surface? A study using an accelerometer attached to all three exploration instruments (finger, real stylus, and virtual stylus) could give further information about the forces and vibrations felt by the participants. These data would have the potential to credit or discredit the idea of damping effects by the fingerpad, as well

as determine whether the vibrations delivered to the participant correlated with the perceived roughness of the surface.

6.3 Conclusions

Two experiments to estimate the amplitude discrimination thresholds for sinusoidal and triangular gratings were conducted using high-definition real and virtual haptic textures. Each experiment consisted of three conditions: using either a finger on a real texture (Finger-real), a stylus on a real texture (Stylus-real), or a stylus on a virtual texture rendered by a force feedback device (Stylus-virtual). The real haptic texture conditions employed stainless steel textured surfaces produced by an EDM process that included post-fabrication polishing. The virtual haptic texture condition used a high displacement-resolution force-feedback device to render virtual gratings with the same profiles as the real textures.

What is emerging from the present as well as previous similar studies is the extraordinary sensitivity of human skin to the vibrations resulting from stroking a surface with micro-geometric height variations, i.e., differences on the order of microns. By conducting parallel experiments with high-definition real textures and virtual surfaces rendered by a high spatial-resolution force-feedback device, it has been shown that, like the magnetic levitation haptic device [23], the ministick is a useful experimental platform for studying human texture perception. Development of the ministick avoids the repeated up-front costs associated with the fabrication of new real stimuli at the initiation of a perceptual study, and eliminates the relatively cumbersome manual exchange of specimens during the experiment when real surface textures are used. Thus, virtual textures rendered by very high performance haptic interfaces open the door to a wide range of studies that otherwise could not have been conducted easily, quickly, or economically (e.g., [20], [23]).

LIST OF REFERENCES

LIST OF REFERENCES

[1] D. Katz, "The world of touch," 1925/1989.

[2] S. Peddamatham, W. Peine, and H. Z. Tan, "Assessment of vibrotactile feedback in a needle-insertion task using a surgical robot," *Proceedings of the 2008 Symposium on Haptic Interfaces for Virtual Environment and Teleoperator Systems*, 2008.

[3] S. M. C. Alaimo, L. Pollini, A. Magazzu, J. P. Bresciani, P. R. Giordano, M. Innocenti, and H. H. Bulthoff, "Preliminary evaluation of a haptic aiding concept for remotely piloted vehicles," *Proceedings of the 2010 international conference on Haptics*, 2010.

[4] C. E. Connor, S. S. Hsiao, J. R. Phillips, , and K. O. Johnson, "Tactile roughness: Neural codes that account for psychophysical magnitude estimates," *Journal of Neuroscience*, 1990.

[5] M. Hollins, R. Faldowski, S. Rao, and F. Young, "Perceptual dimensions of tactile surface texture: A multidimensional scaling analysis," *Perception & Psychophysics*, 1993.

[6] R. L. Klatzky, S. J. Lederman, C. Hamilton, M. Grindley, and R. H. Swendsen, "Feeling textures through a probe: Effects of probe and surface geometry and exploratory factors," *Perception & Psychophysics*, 2003.

[7] S. S. Stevens and J. R. Harris, "The scaling of subjective roughness and smoothness," *Journal of Experimental Psychology*, 1962.

[8] S. J. Lederman and M. M. Taylor, "Fingertip force, surface geometry, and the perception of roughness by active touch," *Perception & Psychophysics*, 1972.

[9] S. J. Lederman, "Tactile roughness of grooved surfaces: The touching process and effects of macro- and microsurface structure," *Perception & Psychophysics*, 1974.

[10] S. J. Lederman, G. Thorne, and B. Jones, "Perception of texture by vision and touch: Multidimensionality and intersensory integration," *Journal of Experimental Psychology*, 1986.

[11] C. E. Connor and K. O. Johnson, "Neural coding of tactile texture: Comparison of spatial and temporal mechanisms for roughness perception," *Journal of Neuroscience*, 1992.

[12] S. J. Lederman, R. L. Klatzky, C. L. Hamilton, and G. I. Ramsay, "Perceiving roughness via a rigid probe: Psychophysical effects of exploration speed and mode of touch," *Haptics-e: The Electronic Journal for Haptics Research*, 1999.

[13] S. Louw, A. M. L. Kappers, and J. J. Koenderink, "Haptic detection thresholds of gaussian profiles over the whole range of spatial scales," *Experimental Brain Research*, 2000.

[14] H. T. Nefs, A. M. L. Kappers, and J. J. Koenderink, "Amplitude and spatial-period discrimination in sinusoidal gratings by dynamic touch," *Perception*, 2001.

[15] J. M. Weisenberger, M. J. Krier, and M. A. Rinker, "Judging the orientation of sinusoidal and square-wave virtual gratings presented via 2-dof and 3-dof haptic interfaces," *Haptics-e: The Electronic Journal for Haptics Research*, 2000.

[16] P. P. Ho, B. D. Adelstein, and H. Kazerooni, "Judging 2d versus 3d square-wave virtual gratings," *Proceedings of the 12th International Symposium on Haptic Interfaces for Virtual Environment and Teleoperator Systems*, 2004.

[17] S. Choi and H. Z. Tan, "Perceived instability of virtual haptic texture. ii. effect of collision detection algorithm," *Presence: Teleoperators and Virtual Environments*, 2005.

[18] L. B. Rosenberg and B. D. Adelstein, "Perceptual decomposition of virtual haptic surfaces," *Proceedings of the IEEE Symposium on Research Frontiers in Virtual Reality*, 1993.

[19] D. A. Lawrence, L. Y. Pao, A. M. Dougherty, M. A. Salada, and Y. Pavlou, "Rate-hardness: A new performance metric for haptic interface," *IEEE Transactions on Robotics and Automation*, 2000.

[20] S. A. Cholewiak, K. Kim, H. Z. Tan, and B. D. Adelstein, "A frequency-domain analysis of haptic gratings," *IEEE Transactions on Haptics*, 2010.

[21] P. Buttolo, D. Kung, and B. Hannaford, "Manipulation in real, virtual, and remote environments," *Proceedings of the IEEE International Conference on Systems, Man, and Cybernetics*, 1995.

[22] B. J. Unger, A. Nicolaidis, P. J. Berkelman, A. Thompson, S. Lederman, R. L. Klatzky, and R. L. Hollis, "Virtual peg-in-hole performance using a 6-dof magnetic levitation haptic device: Comparison with real forces and with visual guidance alone," *Proceedings of the 10th International Symposium on Haptic Interfaces for Virtual Environment and Teleoperator Systems*, 2002.

[23] B. J. Unger, "Psychophysics of virtual texture perception," *Ph.D. Dissertation, Robotics Institute, Carnegie Mellon University*, 2008.

[24] H. Z. Tan, B. D. Adelstein, R. Traylor, M. Kocsis, and E. D. Hirleman, "Discrimination of real and virtual high-definition textured surfaces," *Proceedings of the 14th International Symposium on Haptic Interfaces for Virtual Environment and Teleoperator Systems*, 2006.

[25] A. M. West and M. R. Cutkosky, "Detection of real and virtual fine surface features with a haptic interface and stylus," *Proceedings of the ASME Dynamic Systems and Control Division*, 1997.

[26] S. Greenish, V. Hayward, V. Chial, A. Okamura, and T. Steffen, "Measurement, analysis, and display of haptic signals during surgical cutting," *Presence: Teleoperators and Virtual Environments*, 2002.

[27] M. K. O'Malley and M. Goldfarb, "On the ability of humans to haptically identify and discriminate real and simulated objects," *Presence: Teleoperators and Virtual Environments*, 2005.

[28] Y. Ikei and M. Shiratori, "Textureexplorer: A tactile and force display for virtual textures," *Proceedings of the 2002 Symposium on Haptic Interfaces for Virtual Environment and Teleoperator Systems*, 2002.

[29] K.-U. Kyung, S.-W. Son, G.-H. Yang, and D.-S. Kwon, "How to effectively display surface properties using an integrated tactile display system," *Proceedings of the 2005 IEEE International Conference on Robotics and Automation*, 2005.

[30] G. Campion, A. H. C. Gosline, and V. Hayward, "Does judgement of haptic virtual texture roughness scale monotonically with lateral force modulation?," *Proceedings of the 6th international conference on Haptics: Perception, Devices and Scenarios*, 2008.

[31] R. Samra, D. Wang, and M. H. Zadeh, "Design and evaluation of a haptic tactile actuator to simulate rough textures," *Proceedings of IEEE Virtual Reality 2010*, 2010.

[32] R. Samra, D. Wang, and M. H. Zadeh, "On texture perception in a haptic-enabled virtual environment," *Proceedings of IEEE International Symposium on Haptic Audio-Visual Environments and Games (HAVE 2010)*, 2010.

[33] S. Choi and H. Z. Tan, "Perceived instability of virtual haptic texture. i. experimental studies," *Presence: Teleoperators and Virtual Environments*, 2004.

[34] S. Choi and H. Z. Tan, "Perceived instability of virtual haptic texture. iii. effect of update rate," *Presence: Teleoperators and Virtual Environments*, 2007.

[35] R. L. Klatzky, S. J. Lederman, and V. A. Metzger, "Identifying objects by touch: An expert system," *Perception & Psychophysics*, 1985.

[36] R. L. Klatzky, "The intelligent hand," *The Psychology of Learning and Motivation*, 1987.

[37] M. A. Symmons, "Active and passive haptic exploration of two- and three-dimensional stimuli," *PhD Thesis, Monash University*, 2005.

[38] S. J. Lederman, "Skin and touch," *Encyclopedia or human biology, Volume 8*, 1997.

[39] D. Picard, C. Dacremont, D. Valentin, and A. Giboreau, "Perceptual dimensions of tactile textures," *Acta Psychologica*, 2003.

[40] M. M. Taylor and S. J. Lederman, "Tactile roughness of grooved surfaces: A model and the effect of friction," *Perception & Psychophysics*, 1975.

[41] S. J. Lederman, J. M. Loomis, and D. A. Williams, "The role of vibration in the tactual perception of roughness," *Perception & Psychophysics*, 1982.

[42] E. Gamzu and W. Ahissar, "Importance of temporal cues for tactile spatial-frequency discrimination," *The Journal of Neuroscience*, 2001.

[43] S. J. Lederman and R. L. Klatzky, "Feeling through a probe," *Proceedings of the ASME International Mechanical Engineering Congress: Dynamic Systems and Control Division (Haptic Interfaces for Virtual Environments and Teleoperator Systems)*, 1998.

[44] R. L. Klatzky and S. J. Lederman, "Tactile roughness perception with a rigid link interposed between skin and surface," *Perception & Psychophysics*, 1999.

[45] M. Shimojo, M. Shinohara, and Y. Fukui, "Human shape recognition performance for 3-d tactile display," *IEEE Transations on Systems, Man, and Cybernetics - Part A: Systems and Humans*, 1999.

[46] J. C. Bliss, H. D. Crane, and S. W. Link, "Effect of display movement on tactile pattern perception," *Perception & Psychophysics*, 1966.

[47] D. G. Caldwell, S. Lawther, and A. Wardle, "Tactile perception and its application to the design of multi-modal cutaneous feedback systems," *Proceedings of the 1996 IEEE International Conference on Robotics and Automation*, 1996.

[48] K. Salisbury, D. Brock, T. Massie, N. Swarup, and C. Zilles, "Haptic rendering: programming touch interaction with virtual objects," *Proceedings of the 1995 symposium on Interactive 3D graphics*, 1995.

[49] G. Campion and V. Hayward, "On the synthesis of haptic textures," *IEEE Transactions on Robotics*, 2008.

[50] B. Unger, R. Hollis, and R. Klatzsky, "The geometric model for percieved roughness applies to virtual textures," *Proceedings of the 2008 Symposium on Haptic Interfaces for Virtual Environment and Teleoperator Systems*, 2008.

[51] N. A. Macmillan and C. D. Creelman, "Detection theory: A user's guide," 2004.

[52] M. Kocsis, H. Z. Tan, and B. D. Adelstein, "Discriminability of real and virtual surfaces with triangular gratings," *Proceedings of the Second Joint EuroHaptics Conference and Symposium on Haptic Interfaces for Virtual Environment and Teleoperator Systems*, 2007.

[53] R. Traylor, D. Wilhelm, B. D. Adelstein, and H. Z. Tan, "Design considerations for stand-alone haptic interfaces communicating via udp protocol," *Proceedings of the 2005 World Haptics Conference (WHC05): The First Joint EuroHaptics Conference and the Symposium on Haptic Interfaces for Virtual Environment and Teleoperator Systems*, 2005.

[54] B. D. Adelstein, "Three degree of freedom parallel mechanical linkage," 1998.

[55] R. Steger, K. Lin, B. D. Adelstein, and H. Kazerooni, "Design of a passively balanced spatial linkage haptic interface," *ASME Journal of Mechanical Design*, 2004.

[56] X.-D. Pang, H. Z. Tan, and N. I. Durlach, "Manual discrimination of force using active finger motion," *Perception & Psychophysics*, 1991.

[57] R. T. Verrillo and G. A. Gescheider, "Perception via the sense of touch," *Tactile Aids for the Hearing Impaired*, 1992.

[58] A. J. Brisben, S. S. Hsiao, and K. O. Johnson, "Detection of vibration transmitted through an object grasped in the hand," *Journal of Neurophysiology*, 1999.

[59] J. M. Weisenberger and M. J. Krier, "Haptic perception of simulated surface textures via vibratory and force feedback displays," *Proceedings of the ASME Dynamic Systems and Control Division*, 1997.

[60] J. M. Weisenberger, M. J. Krier, and M. A. Rinker, "Resolution of virtual grating orientation with 2-dof and 3-dof force feedback systems," *Proceedings of the ASME Dynamic Systems and Control Division*, 1998.

[61] J. M. Weisenberger, M. J. Krier, M. A. Rinker, and S. M. Kreidler, "The role of the end-effector in the perception of virtual surfaces presented via force-feedback haptic interfaces," *Proceedings of the ASME Dynamic Systems and Control Division*, 1994.

[62] G. L. Poling and J. M. Weisenberger, "Multisensory roughness perception of virtual surfaces: effects of correlated cues," *Proceedings of the 12th International Symposium on Haptic Interfaces for Virtual Environment and Teleoperator Systems*, 2004.

APPENDICES

A. EXPERIMENTAL DATA

This appendix contains the detailed experimental results for each of the participants presented in this thesis. Please see section 3.4 for specific details on how this data analysis was performed.

Participant 1

A_1		A_2		A_3		A_4	
	73 | 27		98 | 7		93 | 2		103 | 0*
	38 | 62		7 | 88		4 | 101		0* | 97
d'	0.918	d'	2.950	d'	3.806	d'	4.652
$\sigma_{d'}$	0.185	$\sigma_{d'}$	0.269	$\sigma_{d'}$	0.369	$\sigma_{d'}$	0.528
β	0.154	β	0.026	β	0.130	β	0.019

$\alpha =$ 0.241 JND = 4.149

Participant 2

A_1		A_2		A_3		A_4	
	74 | 30		79 | 26		92 | 11		97 | 7
	15 | 81		7 | 88		5 | 92		1 | 95
d'	1.568	d'	2.131	d'	2.874	d'	3.807
$\sigma_{d'}$	0.202	$\sigma_{d'}$	0.234	$\sigma_{d'}$	0.269	$\sigma_{d'}$	0.420
β	-0.226	β	-0.193	β	-0.193	β	-0.407

$\alpha =$ 0.227 JND = 4.402

Participant 3

A_1		
	59	29
	57	55
d'	0.419	
$\sigma_{d'}$	0.182	
β	0.232	

A_2		
	87	4
	5	104
d'	3.393	
$\sigma_{d'}$	0.311	
β	0.010	

A_3		
	96	3
	1	100
d'	4.206	
$\sigma_{d'}$	0.450	
β	-0.227	

A_4		
	118	0*
	0*	82
d'	4.646	
$\sigma_{d'}$	0.529	
β	0.068	

$\alpha =$ 0.234 JND = 4.274

Participant 4

A_1		
	94	6
	7	93
d'	3.031	
$\sigma_{d'}$	0.275	
β	0.039	

A_2		
	90	1
	8	101
d'	3.742	
$\sigma_{d'}$	0.418	
β	0.420	

A_3		
	100	1
	3	96
d'	4.206	
$\sigma_{d'}$	0.450	
β	0.227	

A_4		
	95	7
	1	97
d'	3.805	
$\sigma_{d'}$	0.419	
β	-0.416	

$\alpha =$ 0.363 JND = 2.757

Participant 5

A_1		
	78	23
	37	62
d'	1.068	
$\sigma_{d'}$	0.189	
β	0.212	

A_2		
	95	6
	4	95
d'	3.306	
$\sigma_{d'}$	0.302	
β	-0.093	

A_3		
	106	0*
	0*	94
d'	4.659	
$\sigma_{d'}$	0.527	
β	0.022	

A_4		
	-	-
	-	-
d'	-	
$\sigma_{d'}$	-	
β	-	

$\alpha =$ 0.285 JND = 3.510

Participant 6

A_1		A_2		A_3		A_4	
	77 | 4		98 | 0*		- | -		- | -
	13 | 106		1 | 101		- | -		- | -
d'	2.881	d'	4.656	d'	-	d'	-
$\sigma_{d'}$	0.281	$\sigma_{d'}$	0.528	$\sigma_{d'}$	-	$\sigma_{d'}$	-
β	0.210	β	-0.006	β	-	β	-

$\alpha =$ 0.521 JND = 1.920

Participant 7

A_1		A_2		A_3		A_4	
	95 | 23		111 | 4		95 | 1		- | -
	10 | 72		0* | 85		0* | 104		- | -
d'	2.025	d'	4.084	d'	4.656	d'	-
$\sigma_{d'}$	0.222	$\sigma_{d'}$	0.441	$\sigma_{d'}$	0.528	$\sigma_{d'}$	-
β	-0.153	β	-0.227	β	-0.017	β	-

$\alpha =$ 0.375 JND = 2.669

Participant 8

A_1		A_2		A_3		A_3	
	91 | 2		101 | 0*		- | -		- | -
	4 | 103		0* | 99		- | -		- | -
d'	3.806	d'	4.660	d'	-	d'	-
$\sigma_{d'}$	0.369	$\sigma_{d'}$	0.527	$\sigma_{d'}$	-	$\sigma_{d'}$	-
β	0.121	β	0.004	β	-	β	-

$\alpha =$ 0.614 JND = 1.630

Participant 9

A_1		A_2		A_3		A_4	
	78 | 13		94 | 5		93 | 4		101 | 0*
	45 | 64		31 | 70		18 | 85		13 | 86
d'	1.288	d'	2.145	d'	2.672	d'	3.454
$\sigma_{d'}$	0.203	$\sigma_{d'}$	0.249	$\sigma_{d'}$	0.271	$\sigma_{d'}$	0.405
β	0.424	β	0.568	β	0.400	β	0.607

$\alpha =$ 0.206 JND = 4.861

Participant 10

A_1		A_2		A_3		A_4	
	61 | 39		86 | 17		87 | 9		88 | 0*
	36 | 64		15 | 82		14 | 90		2 | 110
d'	0.638	d'	1.991	d'	2.423	d'	4.382
$\sigma_{d'}$	0.181	$\sigma_{d'}$	0.213	$\sigma_{d'}$	0.235	$\sigma_{d'}$	0.474
β	-0.040	β	-0.021	β	0.107	β	0.091

$\alpha =$ 0.177 JND = 5.656

Participant 11

A_1		A_2		A_3		A_4	
	69 | 39		84 | 18		89 | 8		98 | 5
	22 | 70		8 | 90		8 | 90		1 | 96
d'	1.065	d'	2.323	d'	2.055	d'	3.974
$\sigma_{d'}$	0.189	$\sigma_{d'}$	0.234	$\sigma_{d'}$	0.227	$\sigma_{d'}$	0.430
β	-0.177	β	-0.233	β	0.361	β	-0.328

$\alpha =$ 0.195 JND = 5.122

Participant 12

A_1			A_2			A_3			A_4		
	76	23		103	4		93	2		96	0*
	37	64		17	76		11	94		7	97
d'	1.073		d'	2.687		d'	3.287		d'	3.811	
$\sigma_{d'}$	0.188		$\sigma_{d'}$	0.271		$\sigma_{d'}$	0.335		$\sigma_{d'}$	0.420	
β	0.195		β	0.439		β	0.389		β	0.409	

$\alpha =$ 0.223 JND = 4.480

Participant 13

A_1			A_2			A_3			A_4		
	74	13		98	2		100	0*		97	1
	49	64		33	67		10	90		1	101
d'	1.206		d'	2.494		d'	3.612		d'	4.653	
$\sigma_{d'}$	0.203		$\sigma_{d'}$	0.317		$\sigma_{d'}$	0.410		$\sigma_{d'}$	0.528	
β	0.436		β	0.807		β	0.524		β	-0.008	

$\alpha =$ 0.241 JND = 4.149

Participant 14

A_1			A_2			A_3			A_4		
	74	13		98	2		100	0*		97	1
	49	64		33	67		10	90		1	101
d'	1.206		d'	2.494		d'	3.612		d'	4.653	
$\sigma_{d'}$	0.203		$\sigma_{d'}$	0.317		$\sigma_{d'}$	0.410		$\sigma_{d'}$	0.528	
β	0.436		β	0.807		β	0.524		β	-0.008	

$\alpha =$ 0.241 JND = 4.149

Participant 15

A_1		A_2		A_3		A_4	
83	10	100	6	107	2	106	2
61	46	32	62	17	74	23	69
d'	1.063	d'	1.995	d'	2.979	d'	2.760
$\sigma_{d'}$	0.212	$\sigma_{d'}$	0.238	$\sigma_{d'}$	0.324	$\sigma_{d'}$	0.319
β	0.708	β	0.586	β	0.600	β	0.705

$\alpha =$ 0.187 JND = 5.342

Participant 16

A_1		A_2		A_3		A_4	
51	41	101	5	105	3	-	-
28	80	2	92	0*	92	-	-
d'	0.782	d'	3.702	d'	4.214	d'	-
$\sigma_{d'}$	0.185	$\sigma_{d'}$	0.359	$\sigma_{d'}$	0.451	$\sigma_{d'}$	-
β	-0.255	β	-0.178	β	-0.192	β	-

$\alpha =$ 0.269 JND = 3.715

Participant 17

A_1		A_2		A_3		A_4	
59	47	103	4	100	2	102	1
25	69	9	84	3	95	0*	97
d'	0.767	d'	3.083	d'	3.939	d'	4.657
$\sigma_{d'}$	0.185	$\sigma_{d'}$	0.288	$\sigma_{d'}$	0.383	$\sigma_{d'}$	0.528
β	-0.241	β	0.241	β	0.093	β	0.009

$\alpha =$ 0.239 JND = 4.179

Participant 18

A_1		
	55	45
	15	82
d'	1.142	
$\sigma_{d'}$	0.199	
β	-0.446	

A_2		
	80	22
	0*	98
d'	3.110	
$\sigma_{d'}$	0.399	
β	-0.768	

A_3		
	92	9
	0*	99
d'	3.673	
$\sigma_{d'}$	0.413	
β	-0.490	

A_4		
	84	8
	0*	108
d'	3.719	
$\sigma_{d'}$	0.414	
β	-0.500	

$\alpha =$ 0.243 JND = 4.123

Participant 19

A_1		
	89	16
	18	77
d'	1.906	
$\sigma_{d'}$	0.210	
β	0.073	

A_2		
	92	5
	0	103
d'	3.972	
$\sigma_{d'}$	0.428	
β	-0.356	

A_3		
	92	0*
	0*	108
d'	4.658	
$\sigma_{d'}$	0.528	
β	-0.030	

A_4		
	-	-
	-	-
d'	-	
$\sigma_{d'}$	-	
β	-	

$\alpha =$ 0.363 JND = 2.755

Participant 20

A_1		
	91	14
	9	86
d'	2.423	
$\sigma_{d'}$	0.236	
β	-0.101	

A_4		
	86	0*
	0*	114
d'	4.652	
$\sigma_{d'}$	0.528	
β	-0.052	

A_3		
	-	-
	-	-
d'	-	
$\sigma_{d'}$	-	
β	-	

A_3		
	-	-
	-	-
d'	-	
$\sigma_{d'}$	-	
β	-	

$\alpha =$ 0.475 JND = 2.106

Participant 21

A_1		A_4		A_3		A_3	
97	13	107	0*	-	-	-	-
21	69	0*	93	-	-	-	-
d'	1.912	d'	4.658	d'	-	d'	-
$\sigma_{d'}$	0.213	$\sigma_{d'}$	0.528	$\sigma_{d'}$	-	$\sigma_{d'}$	-
β	0.228	β	0.026	β	-	β	-

$\alpha =$ 0.424 JND = 2.358

Participant 22

A_1		A_2		A_3		A_3	
64	7	96	0*	100	1	-	-
37	92	3	101	1	98	-	-
d'	1.852	d'	4.213	d'	4.653	d'	-
$\sigma_{d'}$	0.235	$\sigma_{d'}$	0.450	$\sigma_{d'}$	0.528	$\sigma_{d'}$	-
β	0.363	β	0.208	β	0.004	β	-

$\alpha =$ 0.367 JND = 2.722

Participant 23

A_1		A_2		A_3		A_4	
66	23	99	0*	100	0*	-	-
29	82	4	97	0*	100	-	-
d'	1.288	d'	4.082	d'	4.660	d'	-
$\sigma_{d'}$	0.192	$\sigma_{d'}$	0.437	$\sigma_{d'}$	0.527	$\sigma_{d'}$	-
β	0.004	β	0.286	β	0.000	β	-

$\alpha =$ 0.325 JND = 3.073

Participant 24

A_1		A_2		A_3		A_4	
	70 | 27		89 | 18		102 | 2		- | -
	7 | 96		2 | 91		0* | 96		- | -
d'	2.079	d'	2.985	d'	4.386	d'	-
$\sigma_{d'}$	0.233	$\sigma_{d'}$	0.326	$\sigma_{d'}$	0.473	$\sigma_{d'}$	-
β	-0.452	β	-0.532	β	-0.123	β	-

$\alpha =$ 0.336 JND = 2.980

Participant 25

A_1		A_2		A_3		A_4	
	62 | 27		98 | 15		89 | 8		100 | 0*
	36 | 75		23 | 64		22 | 81		8 | 92
d'	0.970	d'	1.743	d'	2.183	d'	3.736
$\sigma_{d'}$	0.186	$\sigma_{d'}$	0.207	$\sigma_{d'}$	0.230	$\sigma_{d'}$	0.416
β	0.030	β	0.242	β	0.298	β	0.463

$\alpha =$ 0.175 JND = 5.710

Participant 26

A_1		A_2		A_3		A_4	
	86 | 19		89 | 3		102 | 4		84 | 0*
	53 | 42		47 | 61		22 | 72		35 | 81
d'	0.766	d'	2.007	d'	2.503	d'	2.784
$\sigma_{d'}$	0.192	$\sigma_{d'}$	0.282	$\sigma_{d'}$	0.267	$\sigma_{d'}$	0.400
β	0.529	β	0.841	β	0.526	β	0.873

$\alpha =$ 0.165 JND = 6.060

Participant 27

A_1		
	83	27
	24	66
d'	1.311	
$\sigma_{d'}$	0.193	
β	0.033	

A_2		
	109	2
	36	53
d'	2.338	
$\sigma_{d'}$	0.315	
β	0.928	

A_3		
	87	5
	12	96
d'	2.825	
$\sigma_{d'}$	0.268	
β	0.192	

A_4		
	105	0*
	6	89
d'	3.878	
$\sigma_{d'}$	0.422	
β	0.410	

$\alpha =$ 0.220 JND = 4.554

Participant 28

A_1		
	85	16
	43	56
d'	1.166	
$\sigma_{d'}$	0.197	
β	0.418	

A_2		
	102	12
	27	61
d'	1.757	
$\sigma_{d'}$	0.211	
β	0.374	

A_3		
	100	3
	12	85
d'	3.051	
$\sigma_{d'}$	0.299	
β	0.369	

A_4		
	98	1
	2	99
d'	4.380	
$\sigma_{d'}$	0.473	
β	0.132	

$\alpha =$ 0.208 JND = 4.812

B. PUBLICATIONS

1. H. Z. Tan, B. D. Adelstein, R. Traylor, M. Kocsis, and E. D. Hirleman, "Discrimination of real and virtual high-definition textured surfaces," *Proceedings of the 14th International Symposium on Haptic Interfaces for Virtual Environment and Teleoperator Systems,* 2006.

2. M. Kocsis, H. Z. Tan, and B. D. Adelstein, "Discriminability of real and virtual surfaces with triangular gratings," *Proceedings of the Second Joint EuroHaptics Conference and Symposium on Haptic Interfaces for Virtual Environment and Teleoperator Systems,* 2007.

3. M. Kocsis, S. A. Cholewiak, R. M. Traylor, B. D. Adelstein, D. Hirleman, H. Z. Tan, "Discrimination of Real and Virtual Surfaces with Sinusoidal and Triangular Gratings using the Fingertip and Stylus," *IEEE Transactions on Haptics,* Revised and in review.